

CRC Report No. AV-28-19

**INVESTIGATION OF OPERATIONAL
AND COMBUSTION
CHARACTERISTICS OF THE ASTM
D909 SUPERCHARGE RATING**

Final Report

February 2026



COORDINATING RESEARCH COUNCIL, INC.
1 CONCOURSE PARKWAY • SUITE 800 • ATLANTA, GA 30328

The Coordinating Research Council, Inc. (CRC) is a non-profit corporation supported by the petroleum and automotive equipment industries with participation from other industries, companies, and governmental bodies on research programs of mutual interest. CRC operates through the committees made up of technical experts from industry and government who voluntarily participate. The five main areas of research within CRC are: air pollution (atmospheric and engineering studies); aviation fuels, lubricants, and equipment performance; heavy-duty vehicle fuels, lubricants, and equipment performance (e.g., diesel trucks); light-duty vehicle fuels, lubricants, and equipment performance (e.g., passenger cars); and sustainable mobility (e.g., decarbonization). CRC's function is to provide the mechanism for joint research conducted by industries that will help in determining the optimum combination of products. CRC's work is limited to research that is mutually beneficial to the industries involved. The final results of the research conducted by, or under the auspices of, CRC are available to the public.

LEGAL NOTICE

This report was prepared by Argonne National Lab as an account of work sponsored by the Coordinating Research Council (CRC). Neither the CRC, members of the CRC, Argonne National Lab, nor any person acting on their behalf: (1) makes any warranty, express or implied, with respect to the use of any information, apparatus, method, or process disclosed in this report, or (2) assumes any liabilities with respect to use of, inability to use, or damages resulting from the use or inability to use, any information, apparatus, method, or process disclosed in this report. In formulating and approving reports, the appropriate committee of the Coordinating Research Council, Inc. has not investigated or considered patents which may apply to the subject matter. Prospective users of the report are responsible for protecting themselves against liability for infringement of patents.

Investigation of Combustion and Knocking Characteristics of the ASTM D909 Supercharge Rating

Alexander Hoth, Christopher P. Kolodziej

Argonne National Laboratory, 9700 S. Cass Avenue, Lemont, IL 60439, USA

Keywords: ASTM D909, Aviation Gasoline, Knocking Combustion, Knock Detection

Abstract

The ASTM D909 supercharge rating characterizes the knock resistance of aviation gasoline. Knocking combustion has the potential for catastrophic engine failure and must be prevented in aviation engines. The D909 test method uses a CFR engine in F4 configuration to rate the maximum knock-limited engine load as expressed by the indicated mean effective pressure (IMEP). The D909 method provides a framework of expected IMEP targets for reference fuels. Knocking combustion is an abnormal combustion phenomenon that creates high-frequency pressure oscillations. The D909 test method relies on audible knock detection by the operator to determine the knock limit.

This study performed a literature analysis of the development and specifications of the D909 test method and provides a detailed overview of knocking combustion and knock detection systems. CFR Engines Inc. upgraded its F4 engine with state-of-the-art combustion research instrumentation to allow for detailed combustion and knock characterization. Two sets of tests of D909 conditions were conducted. First, a purely audible unbiased knock detection test was conducted regardless of the framework IMEP targets of the D909 test method, which resulted in higher-than-expected knock-limited IMEP values. Second, the IMEP framework targets of D909 were used without consideration of the perceived knock limit, which resulted in 0% knocking cycles at peak IMEP conditions. Subsequently, while operating under D909 conditions, neither of these two tests met the requirements of the D909 test method due to conflicting requirements. The knock intensity for the performed D909 tests was determined by the maximum

amplitude of pressure oscillations (MAPO) for the installed piezoelectric pressure transducer, an accelerometer-based automotive knock sensor, and a microphone. The knock intensity correlated with $R^2 > 0.7$ across the three sensors. Previous knock detection devices likely suffered from knockless knock measurements which created rating uncertainties and prevented the implementation of knock instrumentation on the CFR F4 engine. This study also includes a thermodynamic analysis of in-cylinder pressure-temperature conditions of standard D909 ratings based on GT-Power simulations.

Table of Contents

Abstract.....	1
Table of Contents.....	3
1. Introduction	4
2. State of the Art.....	6
2.1. Supercharge Rating D909	6
2.2. Aviation Rating D614	12
2.3. Development of Knock Detection Systems	14
2.3.1. Knocking Combustion	14
2.3.2. Knock Detection.....	18
2.4. Summary of the Literature Review.....	28
3. Methodology.....	29
4. Experimental Setup	31
5. Data Analysis of the D909 Test Method.....	36
5.1. Standard D909 Data Analysis	36
5.2. Combustion Analysis	39
5.3. Knock Analysis	46
6. Thermodynamic Modeling of D909 Test Conditions	58
7. Summary.....	65
8. Future Work.....	67
Acknowledgments.....	68
References	68
Abbreviations.....	74

1. Introduction

There are more than 190,000 piston-engine aircraft in the United States. These aircraft spark-ignition (SI) engines operate on aviation gasoline, commonly known as Avgas. The U.S. Energy Information Administration (EIA) tracks the average daily fuel consumption of Avgas, *Figure 1*. While the consumption of Avgas has declined since the 1970s, it has stabilized at approximately 12,000 barrels per day during the last decade, making it a significant fuel market [EIA 2024].

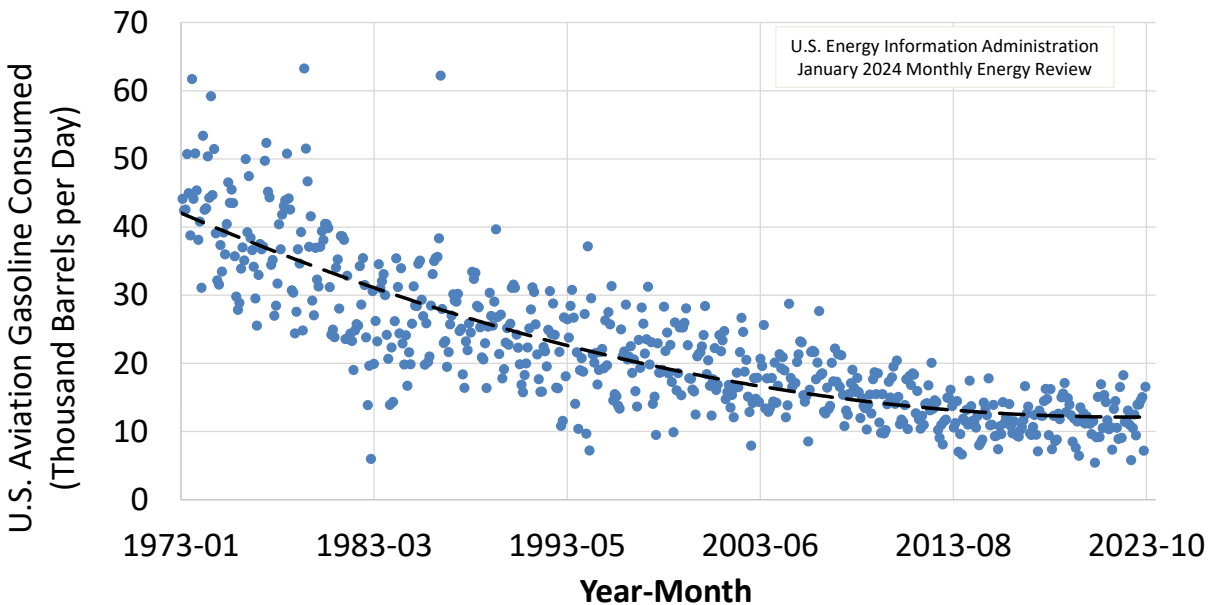


Figure 1. Averaged daily consumption of aviation gasoline in the United States [EIA 2024]

Gasoline properties of Avgas are strictly regulated to ensure adequate performance in aviation SI engines. One of the most critical fuel properties is the fuel’s resistance to knocking combustion as tested by the ASTM D909 “Standard Test Method for Supercharge Rating of Spark-Ignition Aviation Gasoline” and ASTM D2700 “Standard Test Method for Motor Octane Number of Spark-Ignition Engine Fuel” [ASTM D909-2022; ASTM D2700]. Knocking combustion must be prevented in aviation SI engines due to the potential risk of engine failure while in flight. A precise rating of a fuel’s knock resistance is critical to ensure the safe operation of piston-engine aircraft since the fuel is one of the only parts of aircraft operation that is non-redundant.

The Coordinating Research Council (CRC), in collaboration with the U.S. Department of Defense Army and Navy, established the “CRC Rich Mixture Test Procedure for Determining Knock Characteristics of Aviation

Fuels” during World War II [ASTM RR:D02-1986]. Due to the war effort and the critical importance of aviation fuel rating, the initial development effort remained confidential until it was published in 1947 as a tentative D909 supercharged method. While the jurisdiction for the test method has since transferred from CRC to ASTM International with the subsequent ASTM D909 naming, the CRC is interested in characterizing operating conditions and combustion characteristics during standard D909 tests for aviation gasoline.

There are concerns about the future of the D909 test method, given the approximately 10-20 operating F-4 test engines worldwide and limited number of trained operators. In comparison, there are more than 2,000 operators trained on the F-1/F-2 test engines for the ASTM D2699 research octane number (RON) and ASTM D2700 motor octane number (MON) test methods. One potential future pathway for aviation gasoline testing is to extend the D909 test method to allow ratings on a modified F-1/F-2 engine platform. However, there is a significant need for better fundamental understanding of the F-4 engine operating characteristics and the details of the D909 test method.

This report will summarize the origins, conditions, requirements, and rationale of the current ASTM D909 test method. The potential for alternative rating methods for future unleaded aviation gasoline and reference fuels will be identified. This report aims to provide a detailed understanding of the D909 test method as the foundation for potential method upgrades. Operating conditions and combustion characteristics of the D909 test were measured and characterized. Argonne National Laboratory provided expertise in combustion research instrumentation to CFR Engines Inc., who instrumented a standard engine for D909 tests and provided detailed engine combustion measurements. This report discusses detailed combustion and knocking characterization of the test data from CFR Engines Inc. and thermodynamic simulations performed of the pressure-temperature conditions in the combustion chamber during the D909 test method.

2. State of the Art

The ASTM D910 “Standard Specification for Leaded Aviation Gasolines” requires minimum performance number ratings for aviation gasoline. The characterization of the knock resistance and performance number of aviation gasoline are obtained by using the ASTM D909 and the ASTM D2700 test methods, respectively. The two test methods rate the performance or octane number of avgas in a Cooperative Fuel Research (CFR) engine but the operating conditions and test procedure differ. This report mainly focuses on the D909 supercharge test method and its operating conditions. Background information for the D2700 test method is provided as well. This chapter also provides a detailed explanation of knocking combustion and discusses available knock detection instrumentation.

2.1. Supercharge Rating D909¹

The ASTM D910 specification for leaded aviation gasoline requires a minimum D909 Supercharge Rating of 130.0 [ASTM D910, ASTM D909-2022]. The D909 supercharge rating represents the fuel’s resistance to knock during peak power and takeoff conditions. Knock is an abnormal combustion phenomenon, which must be prevented due to the potential for catastrophic engine failure. *Section 2.3.1* provides a detailed description of knocking combustion. The D909 supercharge rating is performed on a CFR engine in the F4 configuration. The CFR F4 engine is a single-cylinder spark-ignition engine with a fixed compression ratio of 7:1. *Table 1* provides an overview of key D909 engine operating conditions. This study summarized operational parameters of the D909 supercharge rating method but the reader is referred to the published ASTM method for full details of the procedure [ASTM D909-2022]. As the name suggests, the F4 supercharge rating enables knock resistance characterization at increased intake pressures. The CFR F4 engine operates at an engine speed of 1,800 rpm, a high engine coolant temperature of 375°F (191°C), and typically rich fuel-air ratios. For comparison, a 1980 Cessna 152 with a Lycoming engine reaches peak horsepower at 2,550 rpm. The air-cooled aircraft engine usually operates at high cylinder temperatures and has a maximum oil temperature of 245°F (118°C) [Cessna 152]. During takeoff and climb, the mixture of piston aircraft engines is typically set to maximum rich conditions for peak power. The D909 test method is designed to replicate highly supercharged piston aircraft engine operation during rich peak power requirements in terms of temporal and thermodynamic cylinder conditions. While the research

¹ Parts of this section were previously published in [Hoth 2024]

octane number (RON) and motor octane number (MON) ratings are interpolated based on the knock intensity of the sample fuel relative to two primary reference fuels, the D909 supercharge method rates the maximum knock-limited power as expressed by the indicated mean effective pressure (IMEP) at incipient knock conditions. The IMEP is calculated as the difference between the brake mean effective pressure (BMEP) and the friction mean effective pressure (FMEP) as shown in Eq. 1 [ASTM D909, 2022]. The BMEP characterizes the engine load during firing operation and is measured via a load cell with a defined lever, while the FMEP is measured the same way but at motoring conditions in which the fuel flow is paused.

$$IMEP = BMEP + FMEP \quad \text{Eq. 1}$$

Table 1. Overview of operating conditions of the ASTM D909 Supercharge Rating Method [ASTM D909]

Parameter	D909 Supercharge Rating
Engine Speed	1,800 rpm
Intake Temperature	107 °C upstream of the fuel injector
Coolant Temperature	191°C
Fuel Delivery	Fuel injection with fuel-air ratio sweep
Intake Pressure	Variable from slightly throttled to supercharged, increased until knock limit is reached
Knock Limit	Incipient knock as determined by operator’s hearing
Engine Load	Peak knock-limited engine load for a given fuel-air ratio

The fuel’s resistance to knock is rated relative to reference fuels. For reference fuels with octane numbers up to 100, the volumetric composition of iso-octane in a binary blend with n-heptane determines its octane number. Since aviation gasolines generally have high knock resistance for reliable operation in piston aircraft engines, their octane number often exceeds that of iso-octane, which has a defined octane number of 100. Therefore, all ratings up to 100 for D909 testing are termed “octane numbers,” while knock resistance exceeding 100 is termed “performance number.” The ASTM D909 test method provides a table of blends with tetraethyl lead in iso-octane to increase its knock resistance. The term performance number originated from the military and is an empirically developed correlation that defines the

performance number relative to the knock-limited IMEP of iso-octane. Therefore, aviation gasoline with a performance number of 130 has a 30% higher knock-limited IMEP than iso-octane [ASTM D909-2022; CFR Inc., 2015A].

The ASTM D909 method defines operation at the lowest audible knock detected by human hearing. This can be a factor in rating uncertainties, especially for identifying light incipient knock amongst different operators. Development efforts of knock detection systems for the CFR F4 engine started in 1939 and intensified in the 1950s. The 1995 published version of D909 lists the Phillips 102-A, M.I.T.-Sperry KM-1, and the Phillips 66 GPI-1 meters as acceptable to aid the audible knock detection but also describes the 102-A and KM-1 devices as obsolete [ASTM D909-1995]. Based on the current approved and published D909 standard from 2022, knock detection is solely performed by the human ear of the operator, and no electronic knock detection system is accepted [ASTM D909, 2022]. More detailed information about the historic development of the knock detection systems is included in *Section 2.3.2*.

The D909 method requires a fuel-air ratio sweep for reference and sample fuels. For a given fuel-air ratio, the knock intensity limits the maximum engine load as determined by the measured IMEP. This is in line with the operation of piston-aircraft engines that usually use rich mixture settings for peak performance during takeoff and climb. For the peak IMEP condition, the knock-limited IMEP of the sample fuel is rated relative to bracketing reference fuels to calculate the performance number. *Equation Eq. 2* shows the interpolation between the IMEP of the sample ($IMEP_{sample}$) and the low ($IMEP_{LOBRF}$) and high bracketing reference fuels ($IMEP_{HIBRF}$). The respective fuel-air ratio for all fuels is determined by the lower bracketing reference fuel ($IMEP_{LOBRF}$). This means that the knock-limited IMEP of every fuel is interpolated at the fuel-air ratio at which the lower bracketing reference fuel reaches its peak IMEP condition.

$$ON_{sample} = \left(\frac{IMEP_{sample} - IMEP_{LOBRF}}{IMEP_{HIBRF} - IMEP_{LOBRF}} \right) * (ON_{HIBRF} - ON_{LOBRF}) + ON_{LOBRF} \quad \text{Eq. 2}$$

As described in the previous paragraph, the fuel-air ratio is a critical measured parameter throughout the D909 test method and defines which knock-limited IMEPs are interpolated. The fuel-air ratio for D909 is the ratio of fuel mass flow divided by the air mass flow. The D909 test method provides a framework of the expected knock-limited IMEP for the reference fuels for a given fuel-air ratio. The fuel-air ratio scale is applicable when the sample aviation gasoline and the reference fuels have a similar stoichiometric

fuel/air ratio, which is dependent on the chemical composition of the fuels. Generally, leaded aviation gasoline is highly paraffinic with added tetraethyl lead (TEL) for added knock resistance. This makes the sample aviation gasoline chemically similar to the paraffinic reference fuels.

Recently, there has been a strong desire to find alternative octane improvers to tetraethyl lead for aviation gasoline due to the negative health impacts of tetraethyl lead [US Treasury Department, 1925; Robert, 1983; Gibbs, 1990; Kitman, 2000; Leake, 1926]. Historic fuels used tetraethyl lead (TEL) to enhance the octane number, but TEL was phased out from use in commercial gasoline in the U.S. in 1973 and eventually banned in 1995 due to its high toxicity [EPA, 1996; Minjares, 2019]. For performance reasons, the combustion of leaded fuels remains for aviation and racing applications while alternatives are being researched [Price, 2019; Sunoco, 2020; Kumar, 2020]. Furthermore, octane ratings beyond 100 require the addition of diluted TEL to iso-octane to be used as reference fuels [ASTM D2699, 2023; ASTM D2700, 2023]. The FAA launched the Eliminate Aviation Gasoline Lead Emissions (EAGLE) initiative to replace leaded aviation gasoline by 2030 [FAA EAGLE]. Removing lead from aviation gasoline requires a highly knock-resistant replacement component.

Some suitable replacement components are ethyl tert-butyl ether (ETBE) or aromatic amines, both of which change the stoichiometric fuel-air ratio of the base gasoline. Aromatic amines change the H/C ratio of the fuel while ETBE (an oxygenated compound) changes both the H/C and the O/C ratio. As shown in *Figure 2*, this has a strong impact on the fuel-air ratio and will result in knock-limited IMEP responses that are shifted relative to that of PRF.

Figure 2 shows the D909 reference fuel framework along with a schematic rating curve of a paraffinic reference fuel or sample fuel (green) and an oxygenated sample fuel (orange). The difference in H/C and O/C ratio shifts the fuel-air ratio of peak IMEP of the oxygenated fuel towards higher fuel-air ratios relative to the paraffinic reference fuels, to the point at which the peak IMEP condition might occur outside of the framework boundaries. The blue dot in *Figure 2* at the peak knock-limited IMEP for the lower bracketing reference fuel determines the fuel-air ratio at which all fuels will be evaluated (blue dashed line). The red dashed line depicts the actual fuel-air ratio for knock-limited IMEP for an oxygenated fuel, which would not be considered during a standard D909 test and can lead to under-rating the performance number. The RON and MON methods resolve this issue by evaluating each fuel independently at its fuel-to-air ratio of highest knock intensity [D2699, D2700].

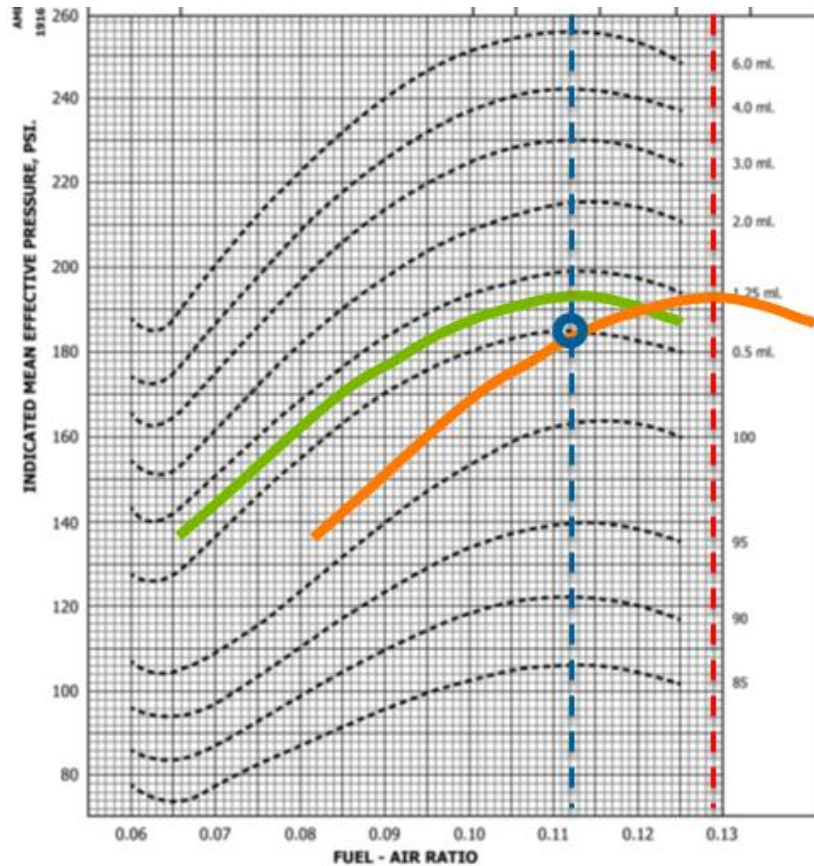


Figure 2. ASTM D909 reference fuel framework with a schematic of a paraffinic fuel (green) and an oxygenated fuel (orange). The blue dot at the peak knock-limited IMEP for the lower bracketing reference fuel determines the fuel-air ratio for which the sample fuel will be rated (blue dashed line). The red dashed line shows the actual fuel-air ratio for the knock-limited peak IMEP of an oxygenated fuel.

The D909 test evaluates the knock-limited IMEP for a variable fuel-air ratio. The orange (oxygenated fuel) curve in *Figure 2* shifted relative to the green (paraffinic fuel) curve because the oxygenated fuel has a reduced stoichiometric air-to-fuel ratio. The stoichiometric air-to-fuel ratio is a fuel property that describes the amount of required air for complete combustion and can be calculated if the fuel chemical composition is known. *Table 2* shows the calculated stoichiometric air-to-fuel ratios for select chemical compounds that are of importance for aviation gasoline rating. Iso-octane and n-heptane are used in reference fuels. Toluene is an aromatic compound with higher knock resistance that would be representative of stoichiometric air-to-fuel ratios of aromatic amines, which have a lower stoichiometric air-to-fuel ratio than that of paraffinic fuels. ETBE is an oxygenated component that is potentially used for future aviation gasoline and has a further reduced stoichiometric air-to-fuel ratio due to an oxygen atom contained in the fuel. Subsequently, the lower stoichiometric air-to-fuel ratio would lead to increased fuel mass flow to achieve stoichiometric combustion compared to paraffinic fuels. This issue can be addressed

by introducing a dimensionless equivalence ratio (ϕ) or excess air-ratio (λ) between the actual air-to-fuel ratio compared to the stoichiometric air-to-fuel ratio, *Eq. 3* and *Eq. 4*. Stoichiometric combustion is defined as $\lambda = 1$ and $\phi = 1$, when there is the correct amount of fuel and air for complete combustion (without excess fuel or air). *Figure 3* depicts the relative quantities of air and fuel in relation to phi and lambda. For rich conditions meaning too much fuel and too little air, $\lambda < 1$ and $\phi > 1$. For lean conditions meaning too little fuel and too much air, $\lambda > 1$ and $\phi < 1$. The equivalence ratio ϕ follows the abscissa of the D909 framework from left/lean ($\phi < 1$) to right/rich ($\phi > 1$). An equivalence ratio-based IMEP evaluation between oxygenated and non-oxygenated fuel as shown in *Figure 2* would prevent the fuel-air ratio shift and is subsequently a better-suited comparison metric when non-leaded aviation gasoline is introduced. Lambda is already a commonly used metric to evaluate automotive gasoline, which can significantly vary in its chemical composition.

$$\lambda = \frac{\text{actual air} / \text{fuel}}{\text{stoichiometric air} / \text{fuel}} \quad \text{Eq. 3}$$

$$\phi = \frac{\text{actual fuel} / \text{air}}{\text{stoichiometric fuel} / \text{air}} \quad \text{Eq. 4}$$

Table 2. Overview of the chemical formula and the respective stoichiometric air-to-fuel ratio for select components.

Fuel	Chemical Formula	Stoichiometric Air-to-Fuel Ratio
Iso-Octane	C ₈ H ₁₈	15.1
N-Heptane	C ₇ H ₁₆	15.15
Toluene	C ₇ H ₈	13.5
ETBE	C ₆ H ₁₄ O	12.8

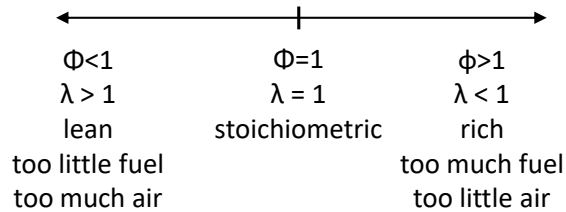


Figure 3. Dimensionless equivalence ratio lambda (λ) and its numeric value for describing air-to-fuel ratio.

2.2. Aviation Rating D614

The octane requirement of aviation gasoline is defined by two ratings: the D909 supercharge rating (discussed in *Section 2.1*) and the D614 lean aviation rating method (discussed in this section). The aviation lean rating was originally published in 1941 as the D614 tentative aviation method, otherwise also known as the aviation lean rating. The method is performed on a CFR engine in F-3 configuration to characterize the fuel's knock resistance under aircraft cruising conditions at lower loads compared to D909. Operational conditions of the CFR F-3 engine are discussed later in this section. Leaded aviation fuel grades such as the commonly used 100LL have a D614 minimum rating requirement of 100 [ASTM D910]. However, D614 was withdrawn in 1970 and is now defined as a correlation to standard MON ratings [ASTM D2700, 2023; ASTM RR:D02-69, 1970; CFR Inc., 2015A, ASTM D910]. The correlation curve was established by the National Exchange Group (NEG) between 1947 and 1964, and is shown in *Figure 4* [ASTM D910, 2021; RR:D02-69, 1970]. For MON ratings up to 100, the performance number had a 1:1 correlation. In the performance number section above 100, the lean aviation rating exceeded the motor octane number.

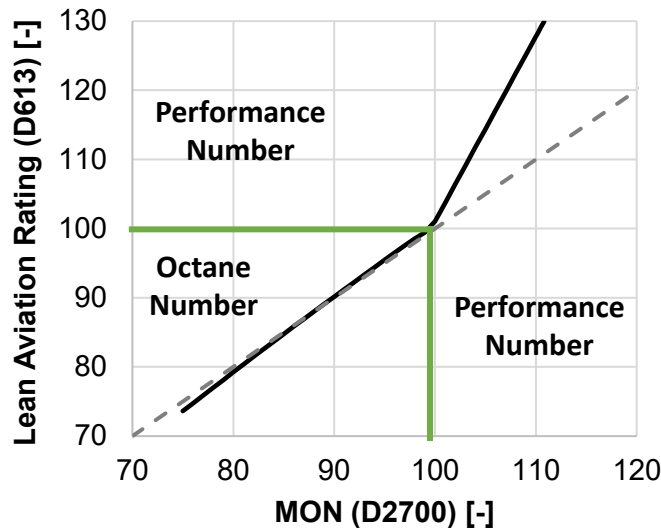


Figure 4. Correlation between the former Lean Aviation Rating (D614) and the Motor Octane Number (D2700) plotted with data from [RR:D02-69; ASTM D2700, 2024].

The correlation between the aviation rating and the motor octane number was not required to retain the same value, thus accepting a correlation curve shown in *Figure 4*. The CFR F-2 configuration for MON ratings is generally similar to the F-3 configuration for aviation ratings. However, it is important to note that operating conditions and the test concept significantly varied between D614 and D2700, cf. *Table 3*. The engine speed, intake temperature setpoint, fuel setting, and knock intensity characterization differ between the two methods. The former D614 test method used the peak thermal plug temperature to rate the knock resistance of sample fuels while D2700 used the peak knock intensity, respectively. The intake pressure setpoint was naturally aspirated for both methods and the same set of reference fuels were used. However, the operating conditions differ significantly between the former D614 and D2700, which does not make them technically equivalent but allows for a conversion between them. The shift from D614 to an already existing D2700 method and only providing a correlation curve as shown in *Figure 4* is not ideal since it is missing technical equivalence. Especially considering upcoming non-leaded fuels, the correlation between D614 and D2700 should be reevaluated for new fuel compositions that might have not been available during the initial correlation study. While not a direct part of this project, the transition from D614 to D2700 provides an example of how methods can evolve based on the needs of the fuel rating industry. A similar approach yet with a higher emphasis on technical equivalence should be targeted for the evolution of D909.

Table 3. Overview of operating conditions for the former D614 Aviation Lean Rating and the ASTM D2700 Motor Octane Number test methods.

Parameter	D614 Lean Aviation Rating	D2700 MON Method
Engine Speed	1,200 rpm	900 rpm
Mixture Temperature	104°C	149°C
Fuel Setting	Adjusted for maximum thermal plug temperature	Set for peak knock intensity, typically rich
Intake Pressure	Naturally aspirated	Naturally aspirated
Knock Intensity	Variable knock intensity based on constant thermal plug temperature	Peak knock intensity determined by D1 Detonation Pickup
Compression Ratio	Variable, depending on knock resistance	Variable, depending on knock resistance

2.3. Development of Knock Detection Systems

This chapter describes the mechanisms that cause knock, and the result of knocking combustion. Measuring knock intensity has been studied for decades and attempts for knock intensity measurement devices for the octane and performance number test are reviewed. The current D909 test method does not list any approved knock detection system and relies on audible knock detection by the operator.

2.3.1. Knocking Combustion²

Knocking combustion is an abnormal combustion phenomenon in SI engines and must be prevented in aviation engines due to its potential for catastrophic engine failure. *Figure 5* shows crank angle-resolved measured cylinder pressure traces from a standard D909 test for iso-octane at peak IMEP conditions. Knocking combustion is characterized by high-frequency pressure oscillations visible in the blue curve in *Figure 5*. The surfaces of the surrounding components of the combustion chamber are usually protected

² Parts of this section were previously published in [Hoth 2024]

by a thin boundary layer that prevents excessive heat transfer from the combustion to the combustion chamber surfaces. The high-frequency pressure oscillations of knocking combustion penetrate the boundary layer and substantially increase local heat transfer to the surfaces of the combustion chamber. The thermodynamic stress from local heat transfer due to pressure oscillations is further escalated by the added mechanical stress from the increased cylinder pressure and pressure rise rates. Excessive knocking combustion can rapidly damage engine hardware such as pistons or piston rings, leading to catastrophic engine failure.

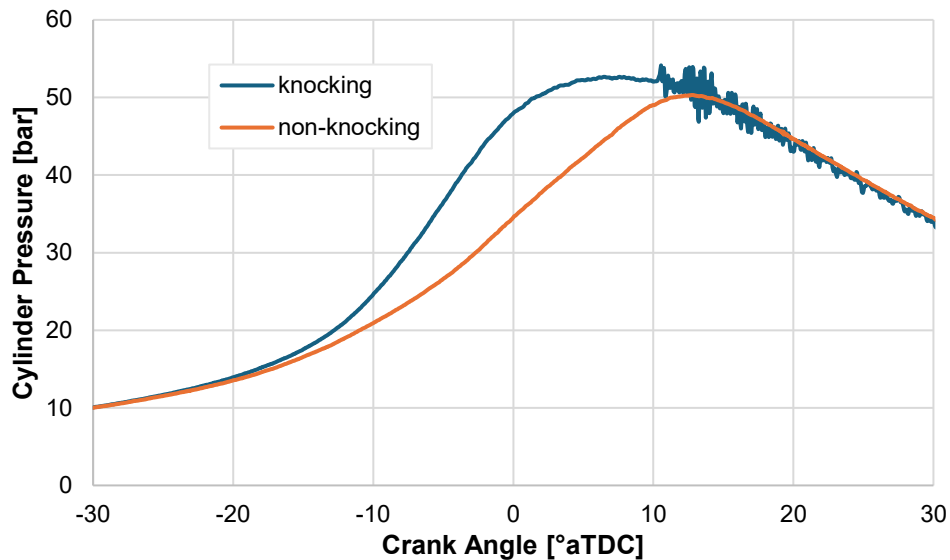


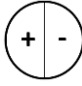
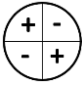

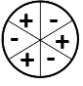
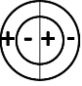
Figure 5. Pressure trace comparison between a knocking (blue) and a non-knocking (orange) case for iso-octane at peak IMEP conditions during a D909 test.

The high-frequency pressure oscillations associated with knocking combustion are caused by local autoignition of the fresh charge. Autoignition causes a rapid local heat release creating a local pressure wave that propagates through the combustion chamber at the speed of sound; the effect is called detonation combustion. The compression shock wave causes adiabatic heating of the unburned fuel-air mixture and subsequent autoignition along the pressure wave [Lee 2008]. Prior to local autoignition, the pressure within the combustion chamber is generally homogeneously distributed. After localized autoignition leads to knocking combustion, the cylinder pressure is no longer uniform. The pressure wave travels at the speed of sound and reflects on the surrounding combustion chamber surfaces. This leads to superimposed pressure oscillations that occur at the resonant frequencies of the combustion chamber. The combustion chamber can be simplified to a cylinder shape and the respective resonant frequencies can be calculated following a procedure published by Dernet et al. [Dernet 2014]. This method is

based on initial discussions by Draper et al. from 1938 [Draper 1938]. Equation Eq. 5 shows the formula for calculating the resonant frequencies as a function of the speed of sound in the numerator and the cylinder bore (B) multiplied by pi in the denominator. The speed of sound can be calculated as the square root of the polytropic coefficient (γ) multiplied by the specific gas constant (R) and the gas temperature (T). The wave number ($\alpha_{m,n}$) is defined for circumferential (m) and radial (n) oscillation modes as provided in Table 4. Table 4 also demonstrates the oscillation modes and the respective calculated resonant frequencies. For the calculations of resonant frequencies, the polytropic coefficient γ was assumed as 1.3 and a cylinder temperature (T_{cyl}) of 2,000 K. The polytropic coefficient was selected lower than most modern engines in alignment with literature values for a CFR engine [Pulpeiro 2019A]. The calculated resonant frequencies of a CFR engine closely align with literature values published by Mittal et al. [Mittal 2009]. Rockstroh et al. found pressure oscillations to start during the initial rapid increase of heat release when measuring cylinder pressure at a 100 kHz sampling frequency [Rockstroh 2018]. The high-frequency pressure oscillations are dampened over time and decay towards the end of the cycle due to friction and the expanding combustion chamber volume.

$$f_{m,n} = \alpha_{m,n} * \frac{\sqrt{\gamma * R * T_{Cyl}}}{\pi * B} \quad \text{Eq. 5 [Dernotte, 2014]}$$

Table 4. Resonant modes and calculated resonant frequencies for a circular cylinder [Dernotte 2014]

Oscillation Mode					
m n	1 0	2 0	0 1	3 0	1 1
$\alpha_{m,n}$	1.841	3.054	3.832	4.201	5.332
Resonant Frequency	6.1 kHz	10.2 kHz	12.8 kHz	14.0 kHz	17.8 kHz

For SI engines, the conventional flame propagation leading up to autoignition has deflagration characteristics. Deflagration combustion happens at subsonic speeds and is governed by diffusion, the reaction rate of the air-fuel mixture, and the turbulence within the combustion chamber [Lee 2008]. These processes vary between cycles, which results in cyclic variations of local temperature conditions leading up to auto-ignition. Subsequently, knocking combustion is a stochastic event. Following conventional

deflagration combustion, autoignition is the first step in creating knocking combustion. The autoignition chemistry of a fuel is dependent on its activation energy and the pressure and temperature history during the compression and combustion process. The autoignition characteristics of a fuel are commonly identified by its ignition delay time as tested in shock tubes or rapid compression machines. Such experimental devices create highly controlled, non-turbulent pressure temperature environments and measure the time delay of a fuel until autoignition. While many fuels exhibit linear relationships in a semi-log plot between ignition delay and pressure-temperature conditions, some fuels such as straight-chain hydrocarbons like iso-octane experience a negative temperature coefficient (NTC) region in which the ignition delay increases or remains constant for increasing temperatures. *Figure 6* depicts ignition delay times taken from Bogin et al. for iso-octane, ethanol, and a 10 vol% blend of ethanol into iso-octane [Bogin 2016]. Ethanol showed an almost linear ignition delay response to changes in temperature. On the contrary, iso-octane had a significant range of temperatures at which the ignition delay remained constant. This difference in ignition chemistry can impact the autoignition and subsequent knocking combustion.

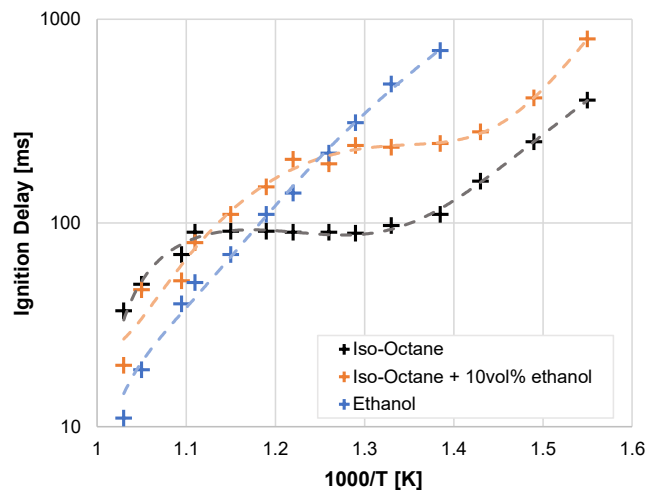


Figure 6. Measured ignition delay curves at 10 bar. Data taken from measurements by Bogin et al. [Bogin, 2016]

Ignition delay is a fuel property and is highly dependent on the pressure-temperature conditions as well as the local air-to-fuel ratio. Subsequently, ignition delay tests are commonly conducted in devices that enable homogenous, non-turbulent testing conditions. Meanwhile, internal combustion engines typically have high turbulence as well as temperature and fuel-air mixture stratification. Autoignition primarily occurs close to the exhaust valve due to the higher local temperatures, which reduces the ignition delay and subsequently results in local autoignition. The cylinder pressure and temperature conditions depend

on many factors such as the intake manifold pressure and temperature, the engine compression ratio, the polytropic coefficient during the compression and expansion stroke, the evaporative cooling from the injected fuel, the residual gas fraction and its temperature, and the heat transfer across the combustion chamber surfaces. The fuel ignition delay impacts the location, quantity, and timing of local autoignition of the fresh cylinder charge. Knocking combustion is caused by local autoignition but not every autoignition ultimately results in knocking combustion. An example of autoignition without knocking combustion is homogeneous charge compression ignition otherwise known as HCCI, which relies on autoignition but does not result in knocking cylinder pressure oscillations.

2.3.2. Knock Detection³

A system to quantify the knock intensity reliably is critical for SI engine operation and during octane number ratings of gasoline. This section will focus on knock detection systems for octane and performance number ratings. While the majority of these knock intensity characterization developments have ultimately only been applied to the RON and MON tests, this historical background provides context for potential future developments of the aviation gasoline rating methods.

Thomas Midgley developed an optical gas engine indicator for early combustion analysis in the years leading up to 1920 [Midgley, 1920]. At this time, knock detection by human hearing was the standard. H.C. Dickinson from the Bureau of Standards developed a so-called Diddle Pin, which used a free pin within a guide in an early attempt at combustion and knock analysis [Boyd, 1946; CFR Inc., 2015]. The Diddle Pin was a qualitative indicator of knock, involving seeing the free pin bounce during knock events, but did not quantify the knock intensity. Thomas Midgley and T.A. Boyd combined Midgley's optical gas engine indicator with Dickinson's Diddle Pin to develop the first version of the bouncing pin, which was presented at the SAE Annual Meeting in 1922 [Midgley, 1922]. *Figure 7* shows the original concept of the bouncing pin as developed in 1922. During knock events, the spring-controlled pin bounced and closed an electrical circuit that illuminated a lamp. The closed circuit also allowed the electrical current to flow through an electrolytic cell filled with diluted sulfuric acid, which created hydrogen. The gas flow was then measured in a graduated cylinder and correlated to the knock intensity. During conventional combustion events, the pin would vibrate but not bounce, subsequently keeping an open circuit and preventing any gas flow. As already suggested by the name, and by the nature of the function principle, the bouncing pin followed

³ Parts of this section were previously published in [Hoth 2024]

the increasing cylinder pressure until knock occurred. The rapid release of heat and subsequent strong pressure rise rate accelerated the pin upward causing it to lose connection to the spring-controlled piston. Therefore, the bouncing pin technically rated the pressure rise rate due to knocking combustion rather than the knock intensity or pressure oscillations itself. Swarts et al. created a dynamic model to simulate the pin movement relative to knocking and non-knocking pressure traces and found the pin to disconnect from the diaphragm for an extended time, rendering it incapable of resolving high-frequency pressure oscillations [Swarts, 2005]. However, in 1922 the understanding of knocking combustion as high-frequency pressure oscillations was not yet known due to a lack of high-frequency cylinder pressure indicating systems. While the bouncing pin allowed some quantitative knock assessment, it remained a relative knock intensity characterization and therefore required knock intensity comparison to reference fuels and reference conditions. Nonetheless, the bouncing pin was an immediate success for rating knock intensity.

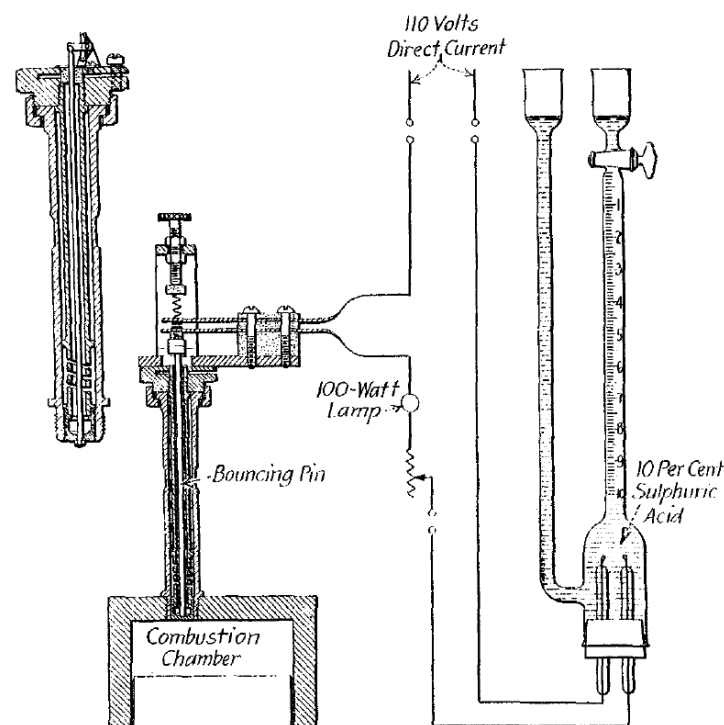


Figure 7. Bouncing pin concept for knock detection in 1922. Reprinted from T. Midgley and T. Boyd originally published by SAE International [Midgley, 1922].⁴

⁴ Figure 7 is reprinted from T. Midgley and T. Boyd originally published by SAE International [Midgley, 1922]. According to the United States Copyright Office Circular 15A, the figure is in the public domain since it was published before 1928.

The original bouncing pin has some limitations that were overcome in the following development process. The spring-controlled piston suffered from blow-by where exhaust components caused the sticking of the pin and a sluggish response. Therefore, the spring-controlled piston was replaced by a steel diaphragm with an equal response [Boyd, 1946]. In 1929, further upgrades were proposed by the Ethyl Corporation Research Laboratory and Weston Electrical Instrument Company, who worked on replacing the gas indicator with an electrical solution. Due to the stochastic nature of knocking combustion, a time-averaged knock intensity measurement was required. In the early bouncing pin, the electrolytic cell was used for integration and quantification of the knock intensity. The upgraded bouncing pin used a current flow through a coil of resistance wire, which generated a voltage in a thermocouple relative to the knock intensity. The output voltage was then visualized as a knock intensity ranging from 0 to 100 in a voltage meter called Knockmeter. The shift from gas-based knock quantification to electrical knock intensity evaluation streamlined the testing and improved its repeatability and reproducibility. Since the knockmeter itself is a basic voltmeter, it is still accepted in the octane test methods today, including its Weston model designation as shown in *Figure 8*. While the knock intensity display changed significantly, the original measurement principle of the bouncing pin remained unchanged by its upgrades [Boyd, 1946; CFR Inc., 2015]. With the publication of the first RON and MON test methods, the bouncing pin was quickly incorporated as the standard instrumentation for rating the knock intensity. This might not have been a surprise since T.A. Boyd collaborated with Thomas Midgley on the first bouncing pin and then served as the chairman of the Cooperating Fuel Research Committee, which created the octane methods [Bartholomew, 1961].



Figure 8. Standard knockmeter for the CFR Engine knock intensity characterization in RON and MON tests.

The first published RON and MON methods used the bouncing pin in combination with a Weston knockmeter scale to characterize the knock intensity [Swarts, 2005]. A couple of years later in 1936, MacCoull used microphone measurements in combination with a frequency analyzer to determine frequencies of knocking combustion. MacCoull found the peak spectral energy to occur at 6.5 kHz for knocking combustion in a standard CFR engine with overhead valves. This closely aligns with the first mode resonant frequency of the CFR combustion chamber, which is approximately 6 kHz, cf. *Table 4* [Draper, 1934; Hoffman, 1961]. MacCoull's finding also validated the findings of Draper, who published the predominant resonant frequency of a CFR engine at 6 kHz [Draper, 1934]. MacCoull furthermore showed that the high-frequency content started only after the spark timing. Therefore, this was one of the first studies to identify knocking combustion as high-frequency pressure oscillations after spark timing and noting that conventional combustion typically occurs at frequencies below 750 Hz. Using a high-pass filter with a cut-off frequency of 375 Hz, MacCoull replicated the bouncing pin knock intensity output, therefore realizing that the bouncing pin rates the pressure rise due to knocking combustion rather than high-frequency oscillations. Since MacCoull was aware of signal disturbances such as dampening from cylinder walls, room acoustics, or differences in measurements depending on the microphone location, he attempted in-cylinder microphone measurements. It was also pointed out that at this early stage of combustion sensor development, a piezoelectric crystal was already known but not yet capable of reliable and accurate pressure measurements at the respective cylinder conditions. MacCoull also identified that his frequency analyzer, the standardized bouncing pin, and the thermal plug all created different knock intensity responses. Furthermore, he noted that a variable lambda as performed in the RON and MON tests does not reflect how engines of that time in 1936 were operated. This subsequently caused offsets between the laboratory knock intensity characterization and on-road fuel performance [MacCoull, 1936].

The first published development of knock detection systems for aircraft engines dates back to an extensive effort by C.S. Draper et al. from the Massachusetts Institute of Technology in 1939. Given the tools available at the time, the research group had a detailed understanding of knocking combustion and developed the first knock detection systems for piston aircraft engines [Draper, 1944]. The developed knock detection system used the combined properties of coils and magnetism to induce a voltage proportional to the velocity of a diaphragm, which made it the first electromagnetic knock detection pickup. During test runs conducted in a CFR engine and aviation engines, the pickup was found to detect high knock intensities but suffered from disturbances from valve motion and conventional combustion [Draper, 1944]. The CRC reported in 1945 regarding aviation methods that no current knock detection system was able to quantify the knock intensity sufficiently and reliably [CRC, 1945]. On the contrary, the

bouncing pin was at that time the universally used knock characterization device for the RON and MON methods [CFR Inc., 2015].

Draper's work on an electromagnetic knock detection pickup set the groundwork for the development of the D1 Detonation Indicator, which was patented by Kenneth Eldredge from the Standard Oil Company in 1942 [US-Patent 2,269,760]. The magnetostrictive sensor has a voltage output proportional to the rate of change of cylinder pressure according to the literature [US-Patent 2,269,760; US-Patent 2,337,522; CFR Inc., 2015; ASTM D2699, 2023]. The outer body of the D1 Pickup is a permanent magnet. A diaphragm at the bottom of the pickup directly faces the cylinder pressure and transfers the forces from the cylinder pressure onto the magnetostrictive center core rod. With no cylinder pressure applied to the center core rod, the crystalline ferromagnets of the magnetostrictive material align with the magnetic field of the outer permanent magnet and do not disturb its magnetic field. *Figure 9A* shows a simplified schematic of the non-stressed magnetostrictive center core rod. Once the cylinder pressure increases, a force is applied to the diaphragm, which slightly flexes and transmits the force to the magnetostrictive center core rod. The applied stress causes the crystalline ferromagnets of the magnetostrictive center core rod to shift toward the least occupied volume, which subsequently alters the magnetic field called the Villari effect. The center core rod is located in the center of a coil as shown in *Figure 9B*. Following Faraday's law, a changing magnetic field within a coil induces a voltage proportional to the velocity of the change. The velocity of the magnetic field change is the first derivative of the deflection of the diaphragm. Furthermore, the deflection is proportional to the mechanical stress, which again is proportional to cylinder pressure. Subsequently, the D1 detonation pickup measures the first derivative of cylinder pressure. With minimal modifications, the D1 detonation pickup invented in 1942 is still in use today for all RON and MON ratings [US-Patent 2,269,760; ASTM D2699, 2023; ASTM D2700, 2023].

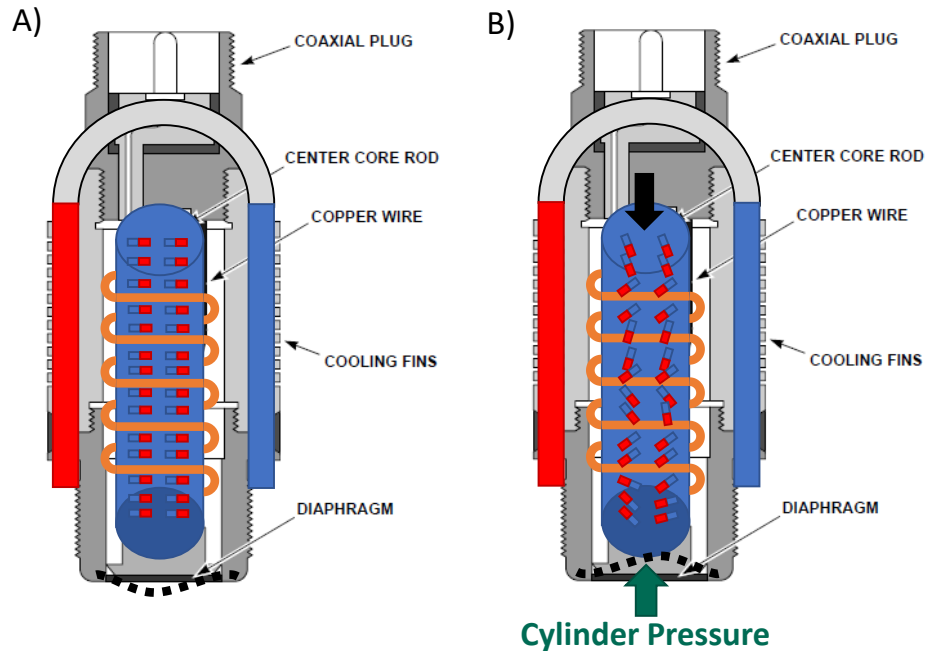


Figure 9. Function Principle of a D1-Detonation Pickup. Reprinted and modified from [CFR Inc., 2015] with permission from CFR Engines Inc.

The D1 detonation pickup is an electromagnetic sensor but its voltage output still requires signal processing to calculate a knock intensity. A follow-up patent by Eldredge provided a possible pathway for knock intensity determination while using the D1 Detonation Pickup but a different Detonation Meter was ultimately selected in the RON and MON methods [US-Patent 2,337,522]. In 1944, Deslonde Boisblanc from the Phillips Petroleum Company submitted a patent application, which was granted in 1948, outlining an analog Detonation Meter to process the output voltage from the D1 Detonation Pickup into a knock intensity value [US-Patent 2,448,323]. The D1 Detonation Pickup output voltage gets routed through an input filter in the Detonation Meter to remove undesired valve noises. *Figure 10A* shows the filter output signal as visualized by Kahler [US-Patent 3,289,461]. The filter type and frequencies have been a topic of further patents and were iterated throughout the development process of the Detonation Meter to replicate the knock ratings of the original bouncing pin [US-Patent 2,448,323; US-Patent 2,496,337; US-Patent 2,633,738; US-Patent 3,289,461; CFR Inc., 2015]. The filtered signal is then passed through a variable threshold amplifier, which the operator modifies to select a threshold between conventional combustion and knocking amplitudes as shown in *Figure 10A* by the red threshold line. The signal portion above the threshold is then passed on to further signal processing in pulse generators and integrators to turn the cyclic nature of the signal into a continuous voltage output. The operator can adjust

the time constant of the integration and further apply an amplitude gain correction for the knock intensity to be displayed on a Weston Knockmeter, as shown in *Figure 8* (p.20). It is noted that this report only provides a general overview of the analog knock signal processing within the detonation meter as it may apply to future aviation gasoline rating methods, and the reader is referred to the respective US patents for further details [US-Patent 2,448,323; US-Patent 2,496,337; US-Patent 2,633,738; US-Patent 3,289,461].

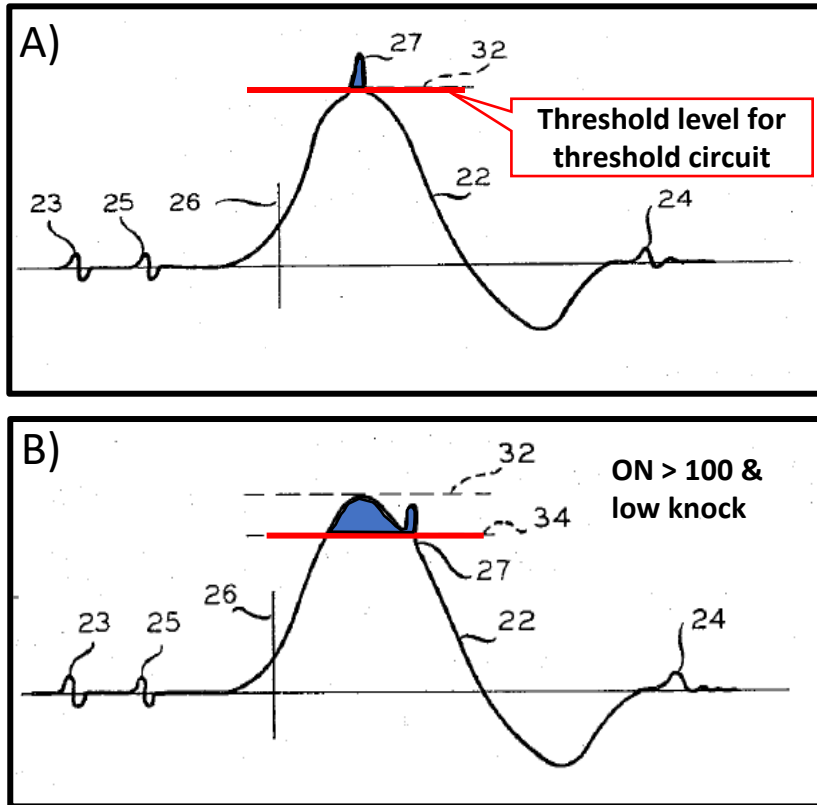


Figure 10. Knock intensity signal processing modified from [US-Patent 3,289,461] showing the variable threshold amplifier selection.

The iterations of the Detonation Meter and the multitude of patents already suggest that the Detonation Meter required upgrades throughout its development process. Nevertheless, the Detonation Meter was first allowed for octane ratings in 1946 [CFR Inc., 2015]. In the 1950s, a new variant Model 501-A Detonation Meter was developed to improve the knock intensity correlation to the original bouncing pin response [CFR Inc., 2015]. Paul Kahler from the Phillips Petroleum Company discussed problems with the Detonation Meter input filter settings in his US patent from 1966, which can lead to a phenomenon termed “knockless knock” [US-Patent 3,289,461]. Depending on the input filter frequencies, the knock intensity output was impacted since the input filter attenuates parts of the D1 signal. Especially for fuels

with an octane number greater than 100, the variable threshold amplifier could select a threshold that contains large parts of the conventional combustion rather than only rating the knocking portion of the cycle. *Figure 10B* visualizes this phenomenon by highlighting the blue area above the red threshold setting. The example trace in *Figure 10B* only shows a similar knocking portion, meaning the actual spike in signal voltage due to knock, compared to *Figure 10A*. However, the blue-marked area is significantly increased due to the inclusion of large portions of the conventional combustion signal. In his 1966 patent, Kahler tried minimizing the issue by installing a band-pass input filter with a frequency range between 500 and 2,500 Hz [US-Patent 3,289,461]. However, it is reiterated from previous findings that the predominant resonant frequency of the CFR engine is based on its cylinder bore diameter, and therefore knocking combustion is at 6 kHz. Therefore, the 501 Detonation meter is blind to high-frequency pressure oscillations that are the most defining characteristic of knocking combustion [Draper, 1934; Hoffman, 1961]. Hoffman elaborated on this detail about the 501 detonation meter in 1961 and showed filtered vs. non-filtered signal traces [Hoffman, 1961]. Furthermore, Hoffman found that benzene with an octane number much greater than 100 showed no pressure oscillations at all during a standard octane test, despite having a measured knock intensity. Therefore, the evaluated knock intensity consisted solely of the conventional combustion portion of the signal rather than actual knocking combustion [Hoffman, 1961]. The current octane rating methods still mention knockless knock [ASTM D2699, 2023; ASTM D2700, 2023].

In the continued development process of the Detonation Meter, further variants were established. In 1969, Waukesha Engines developed the Model 501-T, which again aimed at replicating the bouncing pin ratings [ASTM Manual, 1973; Swarts, 2005; ASTM D2699, 2023]. In 1979, the current version of the Detonation Meter, the model 501-C was developed [CFR Inc., 2015; ASTM D2699, 2023]. According to Swarts et al., the ASTM manual of 1990 first mentioned a low-pass input filter in the signal processing of the new 501-C Detonation Meter [Swarts, 2005]. Furthermore, Swarts presents the filter attenuation response for defined frequencies from the 2001 version of the ASTM RON Method, which showed a significant attenuation for frequencies greater than 5 kHz [Swarts, 2005; ASTM D2699, 2001]. The latest version of the analog Detonation Meter was developed in 2017 [ASTM D2699, 2023].

While knock detection systems for RON and MON ratings were available, the CFR F4 engine was in development but the concepts for knock detection systems were not incorporated until the 1950s. Three knock detection systems were discussed in the minutes of multiple ASTM meetings and personal letter communications [ASTM Minutes, 1954; ASTM Minutes, 1955; Texas Company, 1955; Siegel, 1954, Gulf Oil

Corporation, 1955; Standard Oil Company, 1954]. Previous versions of the D909 Method, like the one published in 1995, outline the Phillips 102-A, M.I.T.-Sperry KM-1, and the Phillips 66 GPI-1 meter as acceptable to aid the audible knock detection but also describe the 102-A and KM-1 as obsolete.

In 1955, the Phillips 103-A detonation meter was described as superior to the M.I.T.-Sperry KM-1 meter in terms of rating stability and durability but it still required modifications, which led to the improved 102-A meter [Texas Company, 1955; Siegel, 1954; Gulf Oil Corporation, 1955]. Mr. MacDonald, the chairman of the June 1955 ASTM D02.01 Section C meeting, indicated, that development efforts were shifted to a new gating-type meter [ASTM Minutes, 1955]. In a letter from 1956, Mr. Baxter from the Waukesha Motor Company described the Phillips 66 GPI meter as “entirely favorable” and its potential to substitute the audible knock detection [Baxter, 1956]. The GPI-1 meter uses a purpose-designed E-1 Detonation Pickup, which was the main contributor to its superior rating behavior [Phillips66, 1956].

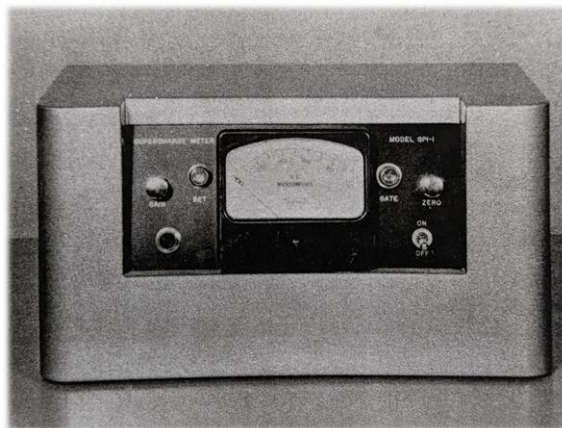


Figure 11. Phillips GPI-1 meter for aviation gasoline knock intensity measurements [Phillips66, 1956].

All meters, however, suffered from fluctuations and sometimes overheating of the E1-Detonation Pickup. The biggest challenge, as already highlighted in the previous section, was the selection of a knock threshold representing the switching point from conventional combustion signal to knocking combustion. Furthermore, sensors tended to overheat due to the high-temperature conditions of the CFR F4 cylinder head from D909 ratings conditions. Therefore, at the current state of the aviation rating D909, knock detection by human hearing is again the only accepted method [ASTM D909, 2022].

While not originally intended for the D909 test method, the ASTM D6424 “Standard Practice for Octane Rating Naturally Aspirated Spark Ignition Aircraft Engines” offers a possible pathway to quantify knock intensity in aviation piston engines [ASTM D6424]. The method uses a piezoelectric pressure transducer

to capture the cylinder pressure trace, similar to the traces shown in *Figure 5* (p. 15). Piezoelectric pressure transducers are designed for high-pressure and high-temperature applications and emit a charge proportional to the pressure change. The electrical charge is then converted in an amplifier to a voltage proportional to the change in cylinder pressure. The D6424 procedure is designed to determine between knocking and non-knocking cycles based on the measured cylinder pressure and the calculated Knock Number. The Knock Number calculation method is visualized in *Figure 12* and evaluates the difference in pressure changes between the expansion and compression stroke. Since knocking combustion has significant high-frequency pressure oscillations, the cumulative pressure change during knock is higher than during non-knocking combustion subsequently leading to higher Knock Numbers. The reader is referred to the ASTM standard for more specific details about the Knock Number evaluation [ASTM D6424].

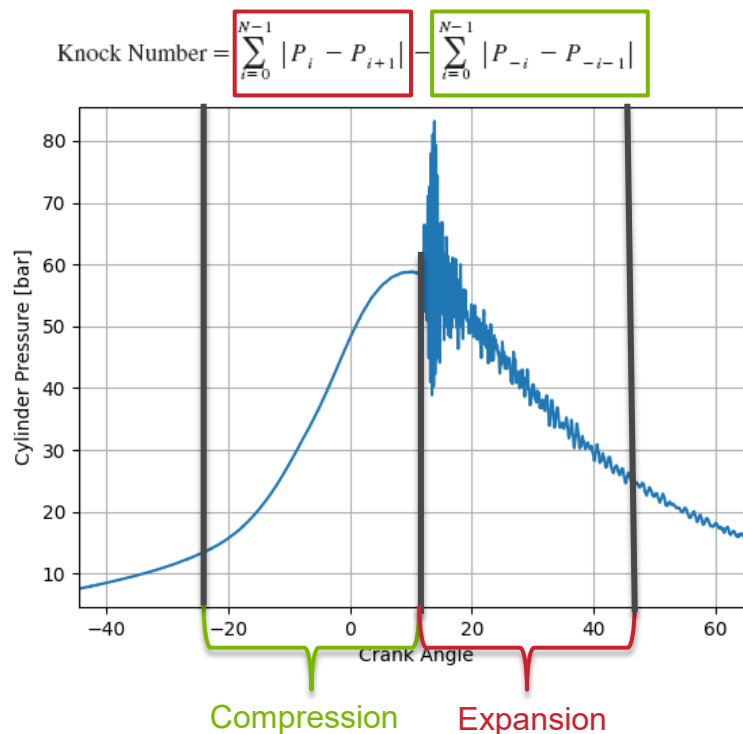


Figure 12. Calculation method of Knock Number per ASTM D6424 for rating the minimum required octane number of aviation engines.

The ASTM D909 Supercharge Rating is evaluated at incipient knock conditions, which the method defines as the “least audible trace knock” and “softest knock that the operator can definitely and repeatedly

recognize by ear although it may not be audible on every combustion cycle (intermittent knock)⁵. This imprecise definition neither provides a specific percentage of required knocking cycles nor a quantitative knock intensity, which provides a range of interpretations. The knocking sound is often described as high-pitch clinking sound similar to how two glass bottles would sound when bounced together. This is in line with the described resonant frequencies of the combustion chamber (cf. *Table 4*, p.16), which are at approximately 6, 10, 13, 14, and 18 kHz. Conventional deflagration combustion is expected to create frequencies below 2 kHz resulting in a much lower pitch. This expected difference in frequencies can be used for knock detection in the D909 method. Based on the definition of knock intensity in D909, it is unclear if a single cycle with high knock intensity is rated differently from numerous cycles with very low knock intensity. This study will investigate the knock detection for the D909 method over a variety of fuels and provide methods to quantify knocking cycles.

2.4. Summary of the Literature Review

Rating the knock resistance of aviation gasoline is critical for reliable SI aviation engine performance due to the potential for catastrophic engine failure due to knocking combustion. The D909 Supercharge Aviation Rating rates the knock resistance of aviation gasoline but relies on audible knock detection by the human operator. Previous methods listed acceptable knock-detection devices with mixed reviews to aid the operator with knock detection but the current D909 method does not allow any knock detection devices. Modern-day knock detection devices could support knock detection and quantify the knock intensity based on the amplitude of pressure oscillations. The push towards unleaded aviation gasoline can create an undesired shift in the knock-limited IMEP curves away from the D909 framework for oxygenated or highly aromatic fuels, which can create undesired rating uncertainties. The dimensionless equivalence ratio ϕ and the air-fuel excess ratio λ were introduced since they are commonly used in automotive combustion research and could better accommodate varying chemical compositions. The transition from D614 to D2700 shows that a change in methods is possible. This study aims to provide the scientific data necessary to guide potential upgrades to the D909 test method.

⁵ Cited from ASTM D909 [ASTM D909]

3. Methodology

The D909 Supercharge Aviation Rating test method rates the maximum knock-limited IMEP of aviation gasoline relative to bracketing reference fuels to calculate a fuel's performance number. The previous chapter provided an overview of the D909 test conditions and outlined the potential for future method upgrades by introducing the dimensionless equivalence ratio ϕ or the air-fuel excess ratio λ . A detailed description of knocking combustion and knock detection systems was also provided. This information will serve as the foundation for the scientific combustion and knock analyses. For this study, CFR Engines Inc., the sole manufacturer of the CFR F4 engine, instrumented their engine with combustion research tools and provided experimental test data of standard D909 tests to CRC. The authors of this study provided guidance for instrumenting the engine to obtain high quality measurements. The state-of-the-art combustion data received from CFR Engines Inc. was analyzed for its combustion and knocking characteristics by this project. An Argonne-developed Python engine combustion post-processing script was developed to perform this analysis following the best practices of modern combustion engine research. This allowed a comparison of the F4 standard dyno-based IMEP measurements to cylinder pressure-based IMEP calculations. The measured test data was analyzed for its knocking characteristics to examine the correlation between audible knock detection and cylinder pressure-based knock detection. Furthermore, a knock threshold was established to determine between knocking and non-knocking cycles to quantify the percentage of knocking cycles for a given D909 test. The knocking characteristics and the cylinder thermodynamic conditions leading to knocking combustion in the D909 method were contrasted to the standard RON and MON tests, which rate the knock resistance of automotive gasoline. The provided data analysis aims to provide the necessary scientific data to guide the future development of the D909 test method.

There are many ways to characterize knocking combustion. Since high-frequency pressure oscillations are the major identifier of knocking combustion over conventional deflagration combustion, this study mainly focuses on calculating the maximum amplitude of pressure oscillations (MAPO), which is a common analysis for automotive SI engine applications. *Figure 13* depicts the cylinder pressure traces from *Figure 5* (p.15), which was measured for iso-octane during a standard D909 test at peak IMEP conditions. The high-frequency pressure oscillations are noticeable for the knocking cycle (blue). *Figure 14* visualizes the calculation procedure for calculating MAPO from the cylinder pressure trace. First, the cylinder pressure is band-pass filtered with cut-off frequencies of 4 kHz and 50 kHz. This attenuates all low-frequency

pressure information from compression, normal deflagration combustion, and expansion while also filtering out high-frequency signal noise above the Nyquist frequency not related to knocking combustion. The filter frequencies were selected based on a study by Rockstroh et al., which showed the dominant knock frequencies in a CFR engine to occur at 6, 10, and 14 kHz [Rockstroh, 2018]. This is also in agreement with the resonant frequency calculations in *Table 4* (p.16). In the second step of calculating MAPO, the crank angle range is truncated to $\pm 60^\circ$ CA around top dead center (TDC) to prevent signal noise from valve events. The bandpass-filtered and truncated signal is then rectified to only include peak-to-average oscillation amplitudes, which are shown as the filtered traces in *Figure 13*. The peak amplitude of the bandpass-filtered, truncated, and rectified signal is termed the maximum amplitude of pressure oscillations (MAPO) and will be the primary knock intensity characterization for this study. The calculation is performed for each individual engine cycle.

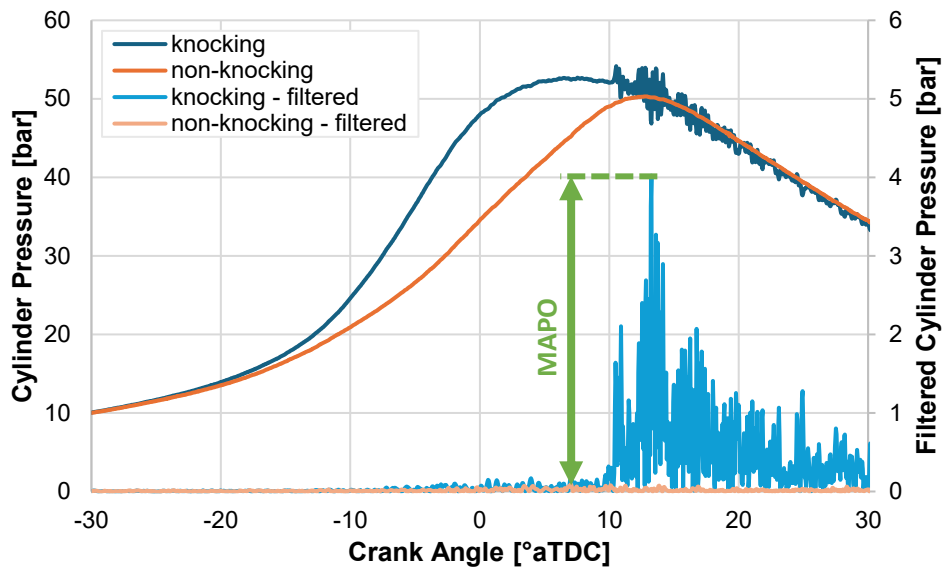


Figure 13. Measured cylinder pressure traces and filtered knock signals during standard D909 tests of iso-octane at peak IMEP conditions.



Figure 14. Calculation procedure for the maximum amplitude of pressure oscillations (MAPO)

4. Experimental Setup

All tests were conducted on a standard CFR F4 engine using the standard D909 test method at CFR Engines Inc. The previous *Section 2.1. Supercharge Rating D909* discussed the details of the D909 test method and CFR engine details. This chapter discusses select engine features and the added combustion research instrumentation as well as details of the fuels that were used for this study.

The CFR F4 engine is a single-cylinder engine operated at 1,800 rpm. It is operated at a coolant temperature of 191 °C due to the unique ethylene glycol water mixture in its cooling system. While the RON (F1) and MON (F2) variations of the CFR engine use a variable compression ratio, the CFR F4 version has a fixed compression ratio of 7:1. The CFR F4 is operated at incipient knock conditions under steady-state conditions for each collected data point. The CFR F4 engine is operated with a compressed air intake manifold that allows intake pressures ranging from slightly throttled to supercharged.

The standard CFR F4 setup already comes with some engine instrumentation to measure critical parameters that must meet D909 specifications. This includes measurements of BMEP and FMEP, the fuel mass flow, the air mass flow, and the respective calculated fuel-air ratio that is critical for the D909 method. The standard instrumentation also measures critical temperatures throughout the intake system and the cooling system to ensure operation within the D909 specifications. The D909 test method has two types of fit for use requirements. The daily fit for use test is achieved by comparing the knock-limited IMEP curve of reference fuels to the D909 framework shown in *Figure 2* (p.10). Another type of fit for use test must be performed after maintenance of the F4 engine and includes the non-knocking IMEP response for a fuel-air ratio sweep at a fixed intake pressure. For this study, both types of fit for use tests were performed and are reported in *Chapter 5. Data Analysis of the D909 Test Method*.

This study aims to analyze the thermodynamic conditions during D909 rating and to characterize the knocking conditions. Subsequently, combustion research instrumentation was added to the standard F4 engine. To retain the standard rating capabilities, none of the instrumentation affected the geometry of the intake, combustion chamber, or exhaust, while also retaining all standard F4 instrumentation. *Table 5* contains a list of all instrumentation additions that were installed by CFR Engines Inc. on their F4 test engine. The intake and exhaust temperatures are recorded at 100 Hz to accurately capture boundary conditions upstream and downstream of the combustion chamber, which is critical to understand the thermodynamic conditions of the engine. The exhaust was also equipped with a wide band lambda sensor

to measure the exhaust gas oxygen concentration, but the very rich operation of the F4 engine, along with the leaded fuels, limited the lifespan of the sensor.

The engine was equipped with an optical crank angle encoder that was data logged at 1 MHz. The high sampling rate is required to get precise crank angle information from the Z, A, and B pulses of the encoder. All additional sensors, except for temperature and lambda, are synchronized with the measured crank angle signal in a custom-developed LabView-based data acquisition system designed by CFR Engines Inc. Piezoelectric cylinder pressure sensors are typically used for automotive knock calibration. The ASTM D6424 for rating the minimum octane requirements for aviation engines also uses a piezoelectric pressure sensor. Subsequently, a Kistler 6054C uncooled pressure sensor was installed in the original knockmeter port as shown in blue in *Figure 15*. A custom-developed adaptor was used to install the sensor flush-mounted in the combustion chamber (red in *Figure 15*) so that the compression ratio remained unchanged. The Kistler sensor has a very high natural frequency of ~ 185 kHz, which reduces the noise interference for the expected high-frequency knock signals and makes it an ideal sensor for knocking characterization. The knocking frequencies from the combustion chamber are transferred as vibrations to the surrounding cylinder head and cylinder liner. Another common way to monitor combustion knock in modern commercial automotive engines is an accelerometer-based knock sensor. These automotive knock sensors are accelerometers that can capture the cylinder head vibrations caused by knocking combustion. The CFR F4 engine was equipped with a typical automotive Bosch knock sensor in addition to the piezoelectric pressure sensor as shown in green in *Figure 15*. These accelerometer-based knock sensors generally offer frequency resolutions between 3 and 25 kHz. The cylinder head vibrations are transferred as audible sound or pressure waves through the air to the ear of the operator. For humans, the ear drums convert the pressure waves to audible sound. Microphones can convert the pressure waves to an electrical signal equivalent to the sound that the operator would hear. Subsequently, a microphone was installed facing the engine and near the engine operator as shown in yellow in *Figure 15*. It is important to note that the microphone is optimized for the human audible range (approximately from 20 Hz to 20 kHz) and has non-linear responses outside of this range. The piezoelectric pressure sensor, the accelerometer, and the microphone are all synchronized to the crank angle encoder and recorded at 216 kHz, which equates to 0.05-degree crank angle resolution. Having all three sensors allows for a comparison of the knocking characteristics as the pressure waves are happening in the combustion chamber, then transition through the cylinder head and cooling channels to the accelerometer, and then further travel through the air to the operator and microphone. The signal transfer from the combustion chamber through the iron cylinder head and the glycol cooling jacket potentially attenuates part of the signal. High-

frequency signals are more rapidly attenuated due to their short wavelength compared to low-frequency signals. Consequently, there is a potential that some of the knock-related frequencies are attenuated before reaching the operator even if the operator has perfect hearing. In addition to cylinder pressure, the crank angle-resolved intake pressure is captured by an installed Kistler 4017A sensor installed close to the intake port. For the crank angle-resolved exhaust pressure, a water-cooled Kistler 4049B was installed close to the exhaust port. The crank angle-resolved intake and exhaust pressure sensors were recorded at 100 kHz.

Table 5. Added combustion research instrumentation to the F4 CFR engine at CFR Engines Inc.

Parameter	Sensor	Sampling Rate
Cylinder pressure	Kistler 6054C with 5010B amplifier	1 MHz / 216 kHz
Intake pressure	Kistler 4017A with 4624A amplifier	100 kHz
Exhaust pressure	Kistler 4049B with 4624A amplifier	100 kHz
Optical Encoder	BEI, HS35	1 MHz
Knock sensor / accelerometer	Bosch 0 261 231 195	1 MHz / 216 kHz
Microphone	Carvin M50	1 MHz / 216 kHz
Wideband lambda sensor	Bosch LSU4.9	100 Hz
Intake port temperature	RTD PT-100	100 Hz
Exhaust temperature	RTD PT-100	100 Hz

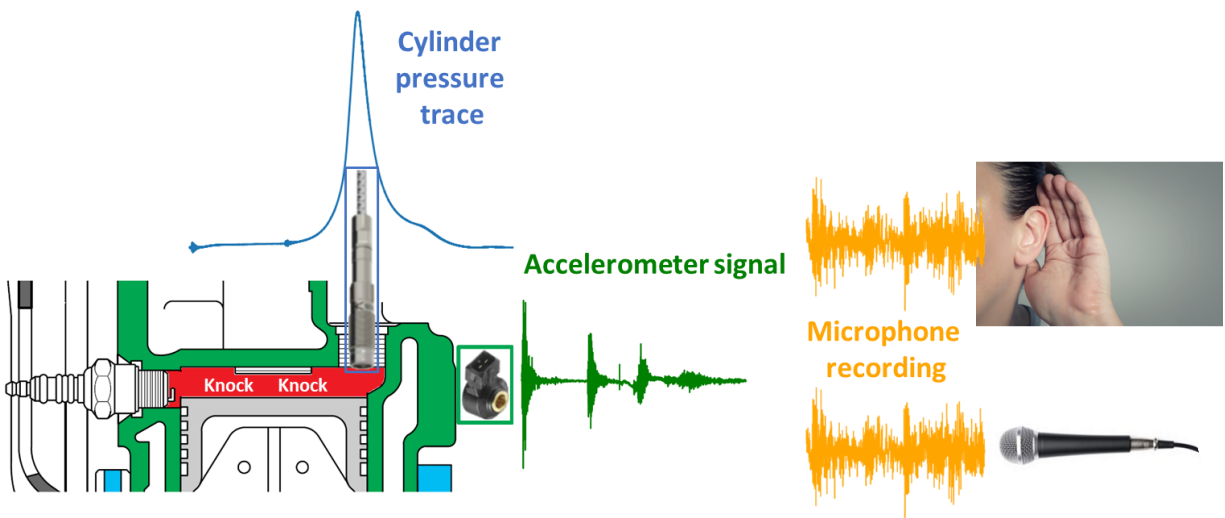


Figure 15. Added combustion research instrumentation to the standard CFR F4 engine and respective signal types.

Figure 15 not only shows the mounting locations of the installed knock instrumentation, but it also shows the respective signals that the pressure transducer (blue), the accelerometer (green), and the microphone (yellow) recorded for an identical combustion cycle. The CFR F4 engine operates on a 4-stroke cycle, meaning it needs two full revolutions (720°CA) to complete intake, compression, expansion, and exhaust strokes. The depicted traces in *Figure 15* are for one complete cycle. The overall shape and amplitudes of the signals differ significantly, which needs to be considered during the post-processing of the knocking characteristics.

CFR Engines Inc. provided the described instrumentation and created a custom-developed LabView-based data acquisition system to record all signals from *Table 5* in addition to the standard D909 instrumentation. The authors of this report provided guidance for the instrumentation and developed a custom Python-based post-processing script. Due to the knock analysis, the sampling rate for knock instrumentation was very high and required automated signal processing. Steady-state operation for 30 seconds resulted in approximately 6.5 million data points per sensor and case. A previous attempt at a reduced 100 kHz sampling rate for the knock instrumentation did not provide the required resolution to accurately capture knocking amplitudes in post-processing. The received test data from CFR Engines Inc. were long arrays of data synchronized with the crank angle in the case of cylinder pressure, accelerometer, microphone, intake pressure, and exhaust pressure. The custom Python processing script first splits the long array of data for each sensor into combustion cycles with constant length. For the 30-second steady-state engine operation at 1,800rpm, this resulted in 450 recorded cycles. In the next step, scaling factors for cylinder, intake, and exhaust pressure were applied to convert the amplifier output voltage into pressure. Piezoelectric pressure sensors measure the pressure change and need an absolute pressure reference. Since a crank angle-resolved intake pressure is available for this study, the cylinder pressure at bottom dead center during the gas exchange was pegged to the measured intake pressure. Bottom dead center was selected since the intake valve is open and the piston temporarily stops. This prevents any airflow and subsequent pressure drops between the intake port and the combustion chamber. The scaled and pegged cyclic data for cylinder pressure, accelerometer, and microphone were then used in *Chapter 5. Data Analysis of the D909 Test Method* for analyzing the combustion and knocking characteristics.

For this study, five fuels were selected with the intention of capturing the widest range of thermodynamic conditions and a representative fuel mixture for aviation gasoline. Subsequently, PRF85 was selected since it is the lowest possible reference fuel in the D909 framework, cf. *Figure 2* (p.10). Iso + 6 ml TEL per US gal. was used since it is the upper limit of the D909 framework. Therefore, PRF85 provides the least intense

thermodynamic conditions while Iso + 6 ml TEL per US gal. results in the highest, respectively. In addition, a national exchange group (NEG) Avgas was selected for this test to include a real-world aviation gasoline. The performance number of the NEG Avgas was expected to match that of Iso+ 1.25 ml TEL per US gal., which is why both were added to the test matrix. PRF100 offers the highest unleaded knock resistance fuel and was added to the test matrix.

Table 6. Overview of the test fuels

Fuel Name	Composition	Octane / Performance Number
PRF85	85 vol% iso-Octane 15 vol% n-Heptane	85
PRF100	100 vol% iso-Octane	100
Iso + 1.25 ml TEL per US gal.	Iso-Octane 1.25 ml TEL per US gal.	129.6
Iso + 6 ml TEL per US gal.	Iso-Octane 6 ml TEL per US gal.	161.0
NEG Avgas	Proprietary	Expected to be similar to Iso + 1.25

5. Data Analysis of the D909 Test Method

The standard CFR F4 engine already has a range of instrumentation to ensure operation within the specification of the D909 test method. This chapter will analyze the standard available test data before performing combustion and knocking characterization of the newly added research instrumentation.

5.1. Standard D909 Data Analysis

The D909 Supercharge Aviation rating requires fit for use tests to ensure engine operation within the specifications of the test method. The previous chapter already summarized the basics of the D909 fit for use requirements. Before any of the actual tests were conducted, the fit for use test after maintenance procedure was followed. For this, fuel-air ratio sweeps for iso + 6 ml TEL per US gal. are performed at a fixed intake pressure of 40 inHG. This generally results in non-knocking conditions but validates that the engine instrumentation and combustion are within the specifications. The maximum measured IMEP was 160 psi, which meets the tolerance (164 ± 5 psi) of the D909 method. In addition to the IMEP, the measured FMEP as an indicator of engine friction was measured at 31.3 psi, which was on the borderline of fit for use for the specific engine operation at 40 inHg intake pressure. The second fit for use requirement is the operation of reference fuels within a $\pm 5\%$ margin of the D909 framework previously shown in *Figure 2* (p.10).

All test fuels for this study were tested under standard D909 test conditions and the respective IMEP results are shown in *Figure 16* in relation to the D909 framework for reference fuels. For the first run of the test method, each fuel was operated at incipient knock conditions as described by the D909 test method. This first test for all fuels was purely based on audible knocking conditions and the operator did not apply the D909 framework for guidance with the respective reference fuel, to prevent any inherent influence on the perceived audible knock intensity. Generally, the fuels followed the expected parabolic shape except for NEG Avgas. The increased knock resistance of fuels as the fuel-air mixture was enriched enabled higher intake pressures leading to increased IMEP before reaching an audible incipient knock condition. As expected, fuels with lower octane or performance numbers allowed for less IMEP before reaching the audible knock limit. It is noted that most of the IMEP data points were above the D909 framework and exceeded the expected knock-limited IMEP by more than the 5% tolerance. However, as mentioned in the beginning of the paragraph, each fuel was operated at its individual audible knock limit

without using the D909 framework to predetermine data points close to the framework. The goal was to explore the actual audible knock limit rather than just relying on the framework. This CFR F4 engine allowed for a higher engine load before reaching the audible knock limit. This is likely due to the vague definition of incipient knock conditions and will be further evaluated in *Section 5.3. Knock Analysis*.

At the richest test conditions, the IMEP of the test fuels noticeably dropped in *Figure 16*. This is generally understood to be misfiring cycles and will be validated in the next section when evaluating cylinder pressure data. The IMEP instrumentation of the F4 is not set up for cyclic analysis and only gives a case-averaged IMEP result. The NEG Avgas did not experience the expected drop in IMEP, which leads to the assumption that it potentially contains some aromatics. As described in *Section 2.1. Supercharge Rating D909*, the chemical composition impacts the stoichiometric air-to-fuel ratio of a fuel and can require increased fuel mass flow for a similar equivalence ratio. The F4 engine was running at peak fuel mass flow and did not allow for a further increase for the richest condition of NEG Avgas. It is expected that a slight increase in fuel mass flow would lead to a drop in IMEP. It is further noted, that the slope of the NEG Avgas IMEP increase with increasing fuel richness is different from that of the reference fuels. This is likely also due to a difference in composition between multi-component Avgas and the purely paraffinic reference fuels. While the official D909 rating of the Avgas is not part of this study, a performance number for the tested Avgas can still be estimated. However, it is noted that the selected PRF brackets are not appropriately spaced for an official performance number calculation. The peak IMEP of the lower bracketing PRF, in this case, iso + 1.25 TEL, determines the fuel-air ratio at which the sample fuel is rated. Since Avgas allowed for a slightly higher knock-limited IMEP than the Iso+1.25TEL reference PRF, the performance number of Avgas exceeds 129.6PN but is much lower than the performance number of iso+6TEL which is 161PN.

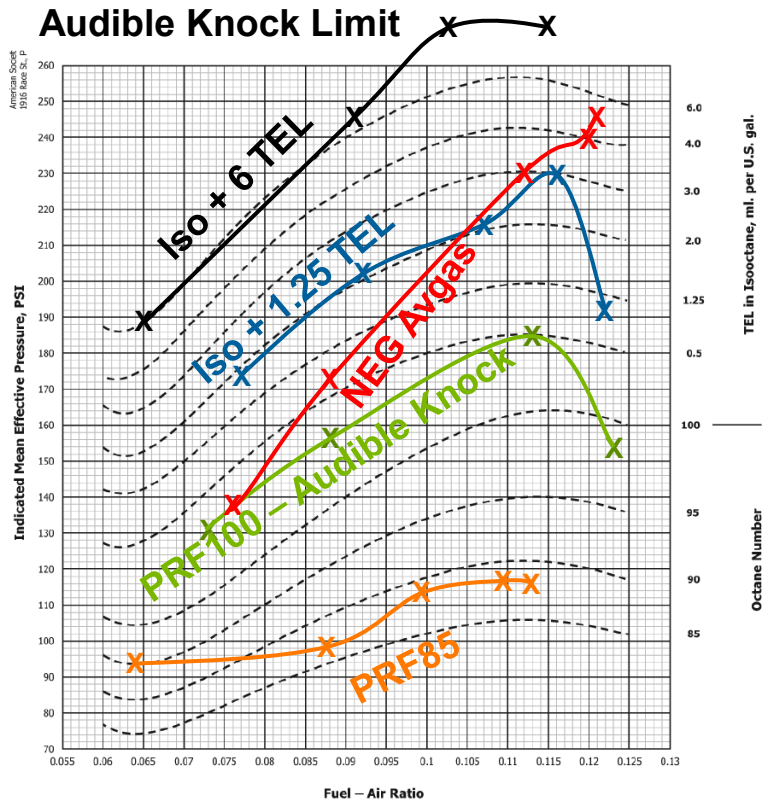


Figure 16. Standard F4 IMEP measurements for all test fuels during fuel-air sweeps tested at audible incipient knock conditions.

The D909 test method has multiple requirements that need to be met for a successful rating of aviation gasoline. In Figure 16, the incipient knock criteria identified by audible knock detection of the engine operator was emphasized. However, as part of the daily fit for use, the IMEP curve for the reference fuels must be within 5% of the D909 framework, which was not the case. Subsequently, a second test for PRF100 was conducted with the specific intention of being close to the D909 framework without consideration of the perceived knock intensity as shown in Figure 17. The “PRF100 framework” dataset was much closer to the D909 framework and meets the daily fit for use criteria. However, especially for the two richest conditions, including the peak IMEP condition, no audible knock was identified by the operator. This can have a significant impact on the rating of performance numbers. These conditions will be of specific interest in the detailed knock characterization in Section 5.3. Knock Analysis.

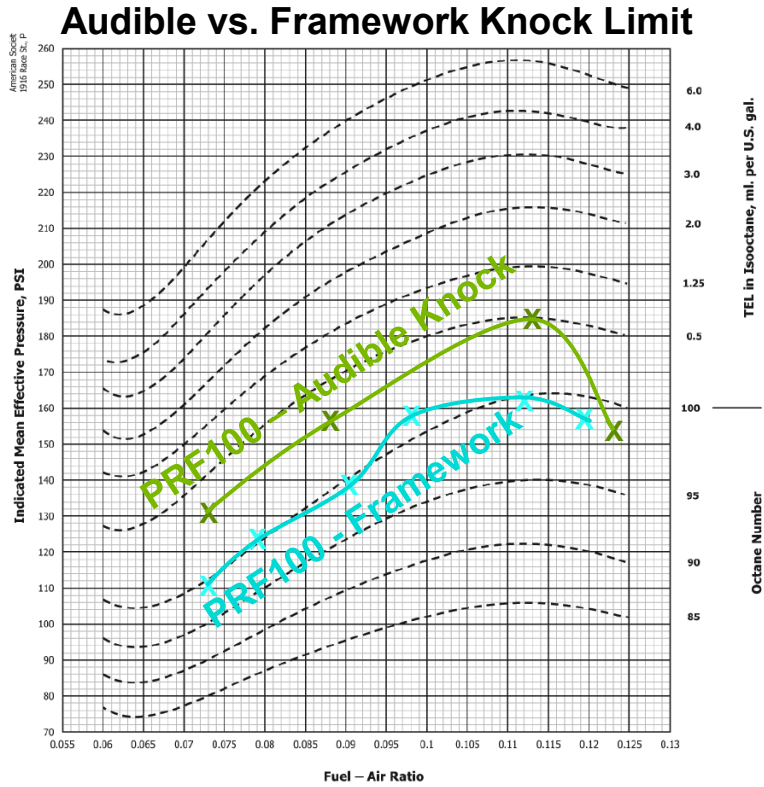


Figure 17. Standard F4 IMEP measurements for PRF100 during fuel-air sweeps tested at 1) audible incipient knock conditions (green) and 2) operation at D909 framework IMEP setpoint (cyan).

5.2. Combustion Analysis

The added piezoelectric cylinder pressure transducer allows for a detailed combustion analysis of the D909 test method. This is a typical process during engine combustion research and automotive engine calibration. Before any combustion-related measurements were performed, a simple check of the thermodynamic loss angle (identified as the crank angle of the peak pressure during motoring conditions) validated the correct crank angle reference. For this engine, the thermodynamic loss angle was found at 0.8 degrees before top dead center ($^{\circ}$ bTDC), which was in the expected range. The motoring peak pressure occurred slightly before reaching top dead center due to heat transfer from the warm compressed air to the surrounding surfaces of the combustion chamber. Another pathway to validate a correct crank angle encoder reference and correct scaling of cylinder pressure is by evaluating the shape of the compression and expansion stroke in a logP-logV diagram. *Figure 18* depicts a measured cylinder pressure trace for PRF100 at peak IMEP conditions in a logP-logV diagram, which has the four strokes and the piston

movement direction indicated. The almost fully parallel lines between the compression and expansion stroke validate the correct settings of the cylinder pressure instrumentation. Furthermore, the correct pegging between intake and cylinder pressure at bottom dead center (BDC) of the gas exchange is validated since the intake and cylinder pressures matched.

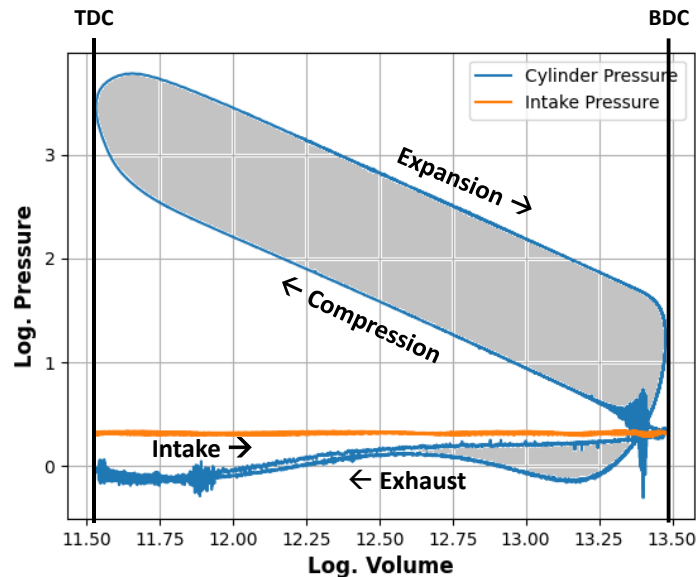


Figure 18. LogP-LogV diagram of a representative pressure trace (blue) and the respective intake pressure (orange). The top (TDC) and bottom dead center (BDC) are marked along with the four strokes and direction of piston movement.

The cylinder pressure transducer provides detailed information about the progression of the combustion event. From the cylinder pressure trace, several parameters can be calculated. Simple ones include the peak pressure of each combustion cycle and the maximum pressure rise rate. Another common calculation is the rate at which heat is released by combustion. From the start of combustion or ignition timing, a cylinder pressure trace deviates from a respective motoring trace by the amount of heat that is released. Since the volume of the combustion chamber is known, the additional cylinder pressure during combustion beyond that of a motoring trace is a result of the combustion and can be calculated. The rate of heat release was integrated to receive the mass fraction burned, which indicates the cumulative percentage of released heat on a crank angle basis for each cycle. Figure 19 depicts the cylinder pressure and respective mass fraction burned trace for a measured cycle for PRF100 operated at peak IMEP conditions. The constant spark timing at 45° bTDC is highlighted in the plot. Furthermore, the crank angle locations of 10%, 50%, and 90% mass fraction burned (CA10, CA50, CA90) are depicted. These parameters are commonly used to evaluate engine combustion. The CA10 usually serves as indicator of the start of

combustion since it can be identified more reliably and repeatable than any lower mass fraction burned values. The CA50 is the center of combustion at which half of the combustion heat is released. The CA50 is a great indicator of combustion phasing and a critical parameter for modern engine calibration since it has a great influence on engine efficiency. The CA90 commonly serves as an indicator for the end of the combustion since the rate of heat release slows down significantly and higher mass fraction burned targets would suffer from significant cyclic variations. The crank angle distance between CA10 and CA90 is called combustion duration and is also commonly used for evaluating the overall combustion. Very short combustion durations are indicators of knocking combustion since the additional flame fronts during knock create a rapid heat release. *Table 7* provides an overview of cylinder pressure-based combustion parameters for all fuels tested at peak IMEP conditions and with audible knock detection as shown in *Figure 16*. As discussed, knocking combustion can impact the combustion duration and subsequently CA50 and CA90. Therefore, the combustion parameters listed in *Table 7* were calculated for each individual cycle and then averaged across 450 consecutive cycles at steady-state operation. While all tested fuels had similar combustion phasing, PRF85 showed delayed combustion phasing.

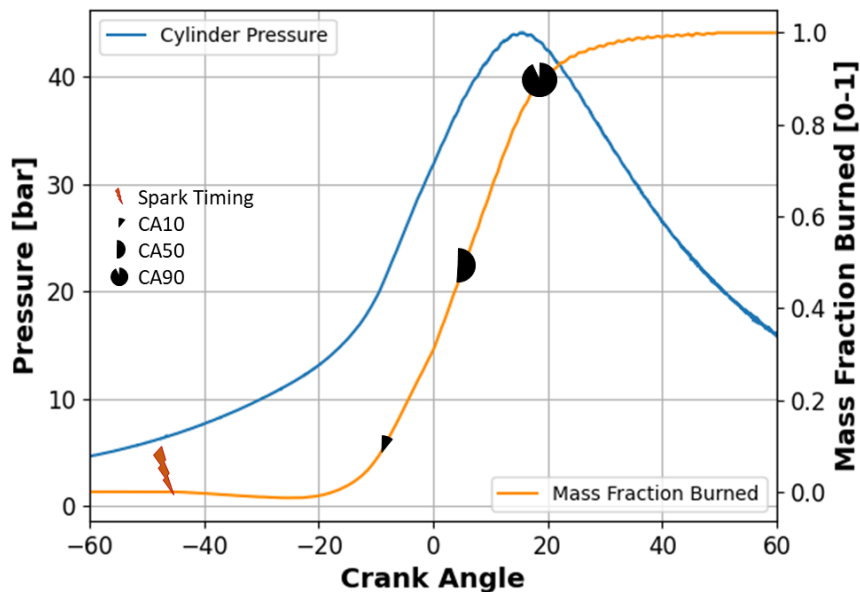


Figure 19. Cylinder pressure and the respective mass fraction burned for a measured cycle of PRF100 at peak IMEP conditions. The spark timing and crank angle degree of 10%, 50%, and 90% mass fraction burned (CA10, CA50 CA90) are depicted.

Table 7. Overview of cylinder pressure-based combustion parameters for all fuels tested at peak IMEP conditions with audible knock detection, cf. Figure 16. The combustion properties are calculated for every individual cycle and then averaged across 450 consecutive cycles at steady-state operation.

Fuel	F/A Ratio	CA10 [°aTDC]	CA50 [°aTDC]	CA90 [°aTDC]	Combustion Duration [°CA]
Iso+6	0.115	-7.2	7.4	19.8	27.0
Iso+1.25	0.116	-3.8	10.7	23.6	27.5
NEG Avgas	0.120	-8.0	6.1	18.1	26.1
PRF100	0.113	-5.9	9.0	22.3	28.2
PRF85	0.109	0.5	16.7	34.0	33.6

The standard IMEP measurement of the CFR F4 engine is based on a load cell and the sum of BMEP and FMEP as shown previously in equation Eq. 1 (p.7). Alternatively, IMEP can also be calculated from cylinder pressure data. Equation Eq. 6 shows the formula for calculating the IMEP based on cylinder pressure (p), the volume trace (V), and the displacement volume (V_d). In general, the work of engine combustion is calculated as the integration of the cylinder pressure over the change of cylinder volume (dV). The work across two full revolutions divided by the displacement volume equals the IMEP of the cycle. The calculation of IMEP can be visualized as the area inside the pressure curve, which is filled in grey in *Figure 18*. Therefore, the IMEP is a direct indicator of the engine load.

$$IMEP = \frac{1}{V_d} * \int_{-360}^{+360} p dV \quad \text{Eq. 6}$$

The cylinder pressure-based IMEP can be calculated for each individual cycle. Similar to the previously discussed combustion parameters, a 450-cycle averaged IMEP can provide a good indication of the engine's operating condition. *Figure 20* shows the calculated cylinder pressure-based IMEP for all fuels tested at audible incipient knock conditions. The IMEP values in *Figure 20* are the identical data points from *Figure 16* (p.38) and follow the same shape and explanation. However, a direct comparison between the two figures reveals an IMEP offset as shown in *Figure 21*. This is due to the substantially different way of calculating IMEP. The CFR F4 load cell measurement relies on separate measurements of BMEP and FMEP. The BMEP is the engine load during firing and the FMEP is meant to characterize the friction of the

engine. However, the FMEP measurement method is not only limited by how it is measuring friction, but is also impacted by the supercharged intake air compared to the ambient pressure exhaust. This pressure differential between intake and exhaust can create a bias of reduced friction for higher performance number fuels tested at higher intake pressures.

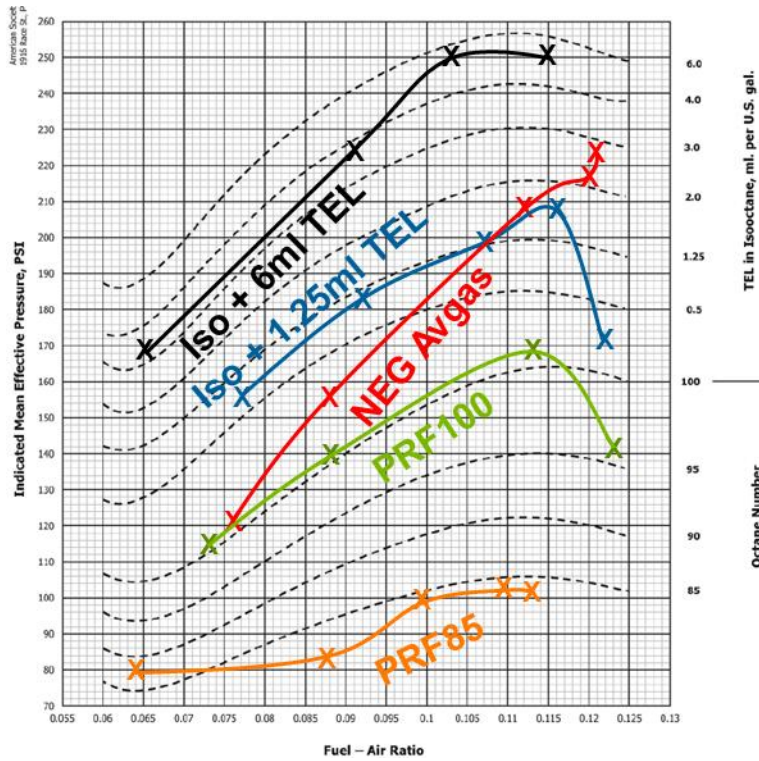


Figure 20. Cylinder pressure-based F4 IMEP measurements for all test fuels during fuel-air sweeps tested at audible incipient knock conditions.

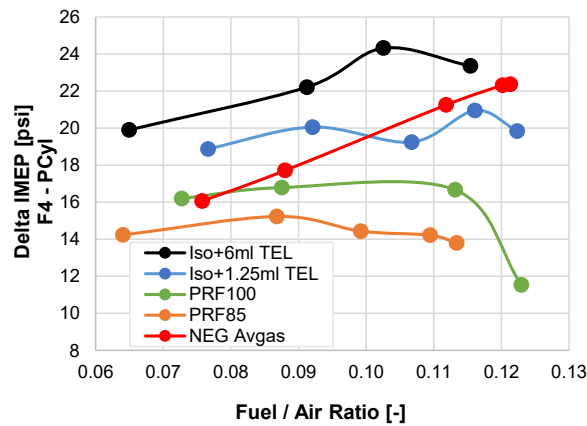


Figure 21. IMEP offset for the cylinder pressure-based (PCyl) IMEP subtracted from the standard dyno-based F4 IMEP.

Figure 22 shows the calculated IMEP offset for the cylinder pressure-based (PCyl) IMEP subtracted from the standard dyno-based F4 IMEP as a function of the measured PCyl IMEP for all data points from Figure 16 and Figure 20. The difference in IMEP measurement technique can create offsets that were found to scale with engine load. The higher engine load was caused by higher intake pressure set points, which caused increased peak cylinder pressures. Subsequently, the IMEP discrepancy also scales with intake pressure and peak cylinder pressures.

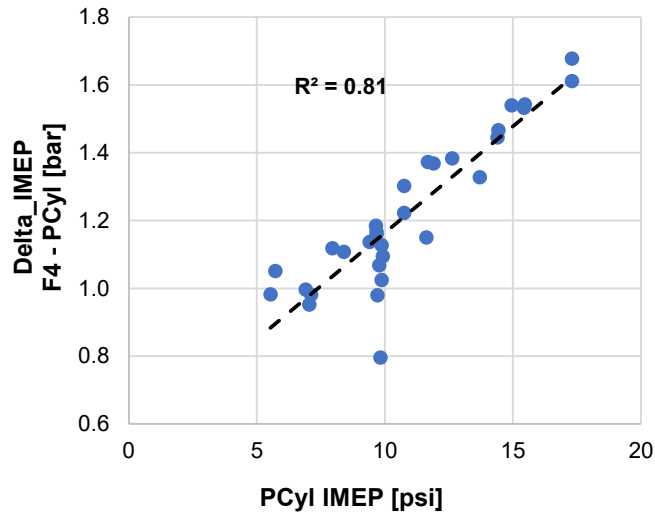


Figure 22. IMEP offset for the cylinder pressure-based (PCyl) IMEP subtracted from the standard dyno-based F4 IMEP as function of measured PCyl IMEP for all data points from Figure 16 and Figure 20.

A great advantage of the cylinder pressure-based IMEP measurement is that it can be performed for each individual cycle and therefore provides statistical information about the cyclic variability of the engine IMEP. Figure 23 depicts the calculated IMEP values for each cycle for PRF100 operated with audible knock detection, cf. Figure 16 (p.38). Four different fuel-air ratios are shown. The least rich condition (black line, F/A 0.073, $\lambda = 0.91$, $\phi = 1.10$) had the lowest overall IMEP output with an average IMEP of 115 psi. An increase in fuel-air ratio increased average IMEP of 140 psi (blue line, F/A 0.088, $\lambda = 0.76$, $\phi = 1.32$). A further increase in fuel-air ratio created the peak IMEP condition at 169 psi (green line, F/A 0.113, $\lambda = 0.59$, $\phi = 1.71$). All three cases discussed so far had low cyclic IMEP variability with a coefficient of variance (CoV) of IMEP less than 3%, which is generally understood as stable engine operation. A further increase in fuel-air ratio reduced the averaged IMEP to 142 psi (orange line, F/A 0.123, $\lambda = 0.54$, $\phi = 1.86$). As can be seen from the orange line in Figure 23, the richest test condition experienced significant cyclic variability in which the IMEP dropped below average and in some cycles to zero (representing mis-fire). This resulted in a coefficient of variance for IMEP of 17% for the richest test conditions. At this fuel-air

ratio, the fuel is operated beyond its ignitability limit, which results in partial burns and misfire events. Recognizing this trend, the cylinder pressure-based calculation of CoV of IMEP could be used as an additional indicator to help the F4 operator more accurately and expediently identify the F/A ratio of peak IMEP during testing of the D909 method, or potential future upgrades to the D909 method.

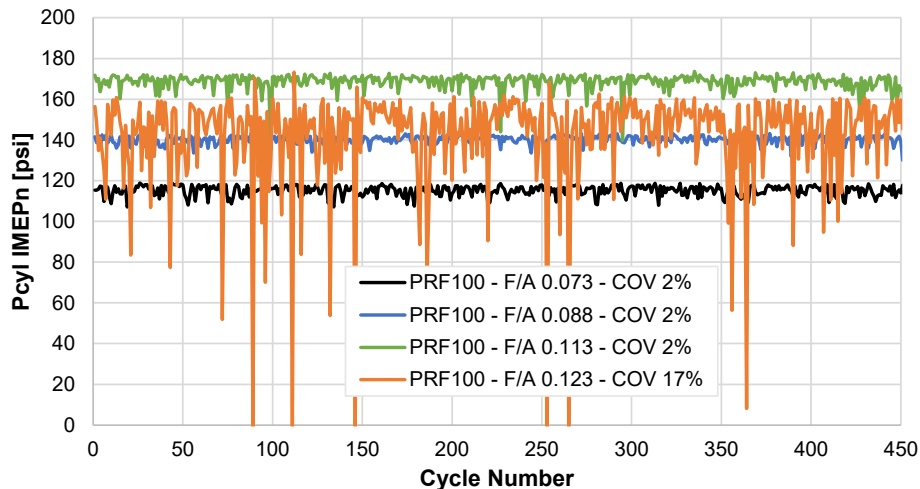


Figure 23. Cyclic cylinder pressure-based IMEP calculations for PRF100 operated with audible knock detection.

The expected partial burns and misfire events from the IMEP analysis for the richest test condition in Figure 23 are validated by the depicted cylinder pressure traces in Figure 24. All cylinder pressure traces are overlaid in transparent grey. Furthermore, an averaged trace (black) is shown for reference. Specifically highlighted in red is cycle 88, which showed a zero IMEP rating in the previous figure. The expected misfire is validated by a cylinder pressure trace that shows no combustion event and follows a motored trace. It is interesting to point out that the very next cycle (cycle 89 in blue in Figure 24) experienced one of the highest knock intensities. This also occurred for other cycles in which a misfire cycle caused a strong knock event for the consecutive cycle. Once a misfire event happens, the residual gas composition in the cylinder is vastly different since no combustion occurred. The additional availability of residual fuel and air can cause the next cycle to have an increased load and strong knocking combustion. Therefore, for the richest test conditions, misfire cycles induced intermittently strong knocking combustion in the subsequent cycle. This is fundamentally different from the knocking events at leaner test conditions, where knock was a stochastic event without an observable trigger. It is also noted that numerous partial burn cycles were observed in the pressure traces shown for this rich test condition in Figure 24. It was pointed out in previous discussions for Figure 16, that the NEG Avgas did not show the IMEP drop at the richest test condition. However, a study of IMEP and cylinder pressure traces revealed

partial burns at the richest test condition. Subsequently, a slightly richer fuel-air ratio would have likely resulted in the expected IMEP drop.

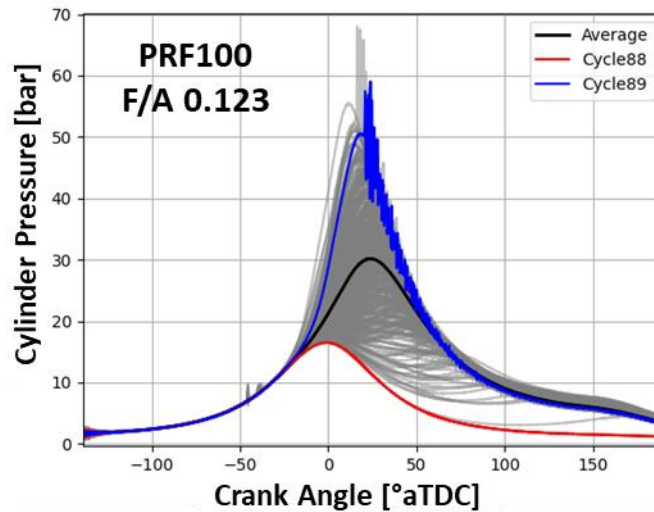


Figure 24. Cyclic variation of PRF100 operated at the richest test condition ($F/A = 0.123$) with audible knock detection (compare orange line in Figure 23). Cycle 88 (red) experienced a misfire. The following cycle 89 (blue) had high knock-intensity.

5.3. Knock Analysis

The characterization and measurement of knock intensity for the D909 method has been a topic of research for many decades. *Section 2.3.2. Knock Detection* reviewed developments of previously available knock detection systems for the D909 method and introduced common knock detection pathways from other aviation and automotive applications. *Chapter 4. Experimental Setup* provided an overview of the available engine instrumentation for this study, which incorporated numerous additional sensors, as shown in *Figure 15* (p.33) and *Table 5* (p.33). For this chapter, the available knock instrumentation is of specific interest. This includes the piezoelectric cylinder pressure transducer, the accelerometer-based automotive knock sensor, and the microphone to capture the entire measurement chain of knock transition from the combustion chamber to the perception of the operator. The signal shape and amplitudes vary significantly between the cylinder pressure, the accelerometer, and the microphone as shown in *Figure 25*, which shows a comparison of the direct measurements for these sensors for PRF100 operated at peak IMEP conditions. The cylinder pressure has high-frequency pressure oscillations overlaid onto a low-frequency oscillation for piston compression and expansion. The accelerometer and the

microphone show low-amplitude oscillations already before knocking combustion starts and subsequent higher oscillations amplitudes following knocking combustion.

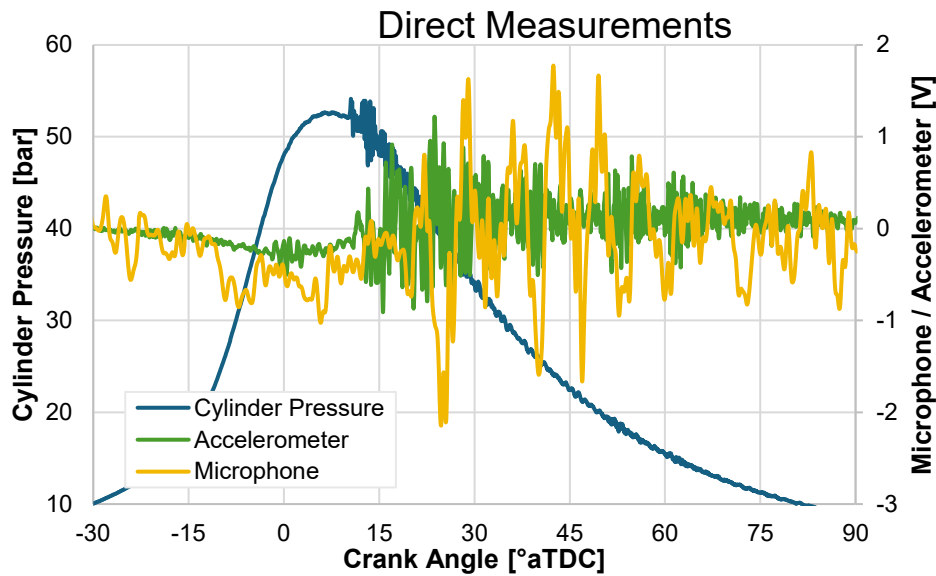


Figure 25. Comparison of direct measurements of cylinder pressure, accelerometer, and microphone signals for an identical knocking cycle for PRF100 at peak IMEP conditions.

The signal shapes differ between sensors, yet a common knock characterization methodology across sensors is desired. The introduced Knock Number from ASTM D6424 (cf. Figure 12, p. 27) is expected to yield good knock intensity characterization for the cylinder pressure signal. However, evaluation of the maximum amplitude of pressure oscillations (MAPO) can provide good knock intensity quantification for all three sensors with the appropriate filtering. Figure 13 (p.30) and Figure 14 (p.30) showed the calculation procedure for MAPO based on cylinder pressure. An identical approach can be applied to the signals from the accelerometer and the microphone. Figure 26 depicts the bandpass-filtered signals for the identical cycles from the previous figure. A bandpass filter with cutoff frequencies at 4 kHz and 50 kHz was used for the cylinder pressure, accelerometer, and microphone. The resulting bandpass-filtered signals show low amplitudes for all sensors until knocking combustion starts. As expected for knocking combustion, the cylinder pressure (blue) showed a rapid increase in pressure oscillations with a high amplitude. The maximum amplitude of the pressure oscillations is termed MAPO PCyl and serves as the knock intensity for cylinder pressure. The amplitude increase for the accelerometer (green) is slightly delayed compared to that of cylinder pressure. This is likely due to the inherent time that the pressure waves need to travel from the gas in the combustion chamber through the cylinder liner and coolant jacket to the side-mounted accelerometer. The peak amplitude for the accelerometer is termed MAPO

Acc. The high amplitudes for the microphone are further delayed compared to the accelerometer. This again is due to the time required for transitioning from the cylinder head to the air and further to the microphone diaphragm. The peak amplitude for the microphone is termed MAPO Mic. Subsequently, MAPO is capable of serving as a knock intensity metric across all three sensors. Nonetheless, comparing the relative knock intensity between the three sensors is not trivial since the measurement chains differ for each sensor.

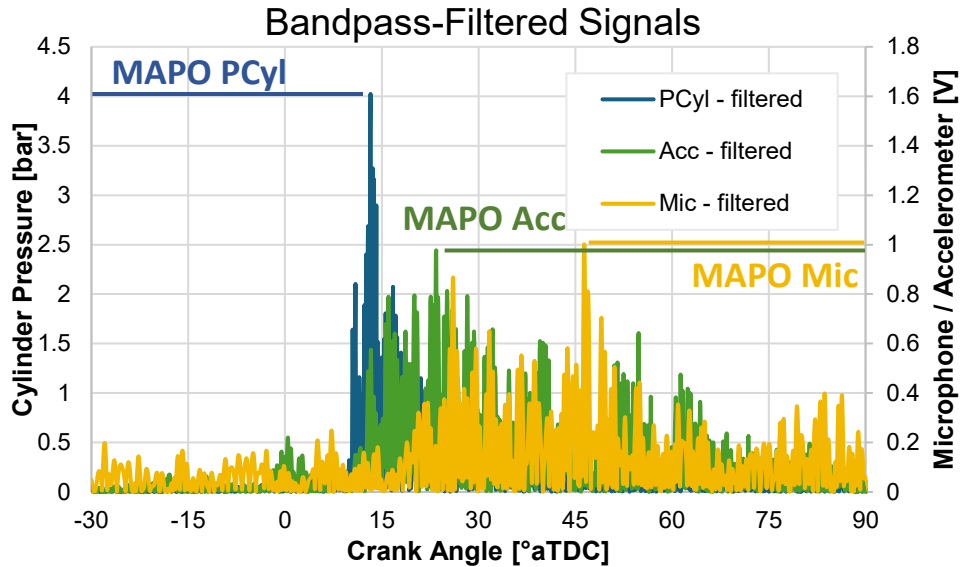


Figure 26. Comparison of bandpass-filtered cylinder pressure (PCyl), accelerometer (Acc), and microphone (Mic) signals of the same knocking cycle for PRF100 at peak IMEP conditions. The respective maximum amplitude of pressure oscillations (MAPO) is also depicted as quantification of knock intensity.

The MAPO analysis for cylinder pressure, accelerometer, and microphone was conducted for each individual cycle for all 450 consecutive cycles. Figure 27 shows a comparison of MAPO knock intensities for PRF100 operated at peak IMEP conditions and audible knock limit for the first 100 cycles. The stochastic nature of knock is pointed out as there is no clear indication of any pattern. The relative amplitude comparison is possible but a study for the overall correlation between sensors is required. It can be seen from the cyclic comparison, that cycles with high MAPO PCyl usually resulted in high MAPO Acc values. Due to the low MAPO Mic amplitudes, a clear indication is not immediately possible but will be part of the next analysis.

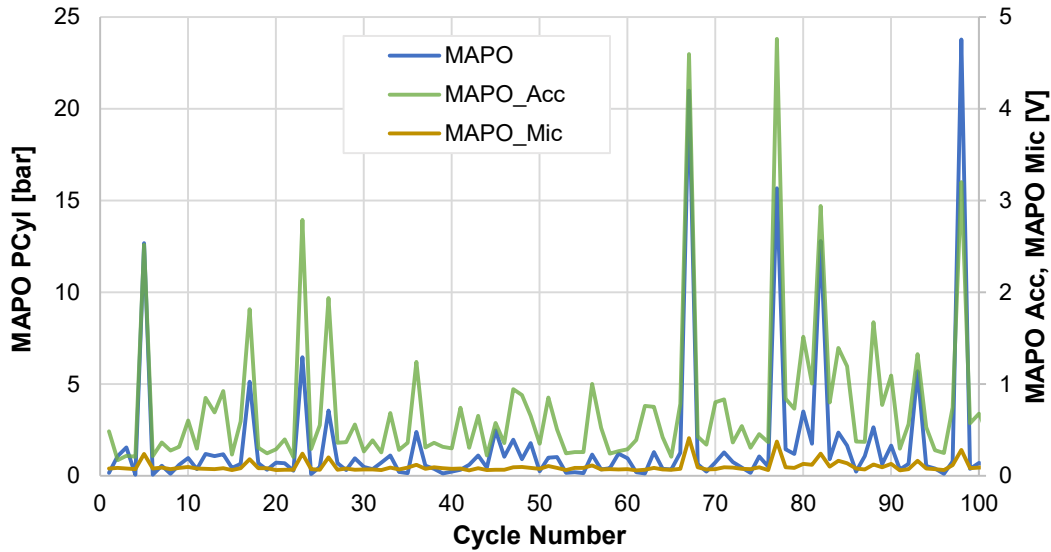


Figure 27. Cyclic MAPO comparison between cylinder pressure, accelerometer, and microphone for PRF100 operated at peak IMEP and the audible knock limit.

Correlating the MAPO knock intensities between cylinder pressure, accelerometer, and microphone is important to understand potential sensor-specific limitations. Figure 28 shows a comparison of MAPO Acc (left-side plot) and MAPO Mic (right-side plot) to MAPO PCyl for 450 consecutive cycles of PRF100 operated at peak IMEP and audible incipient knock. Generally, there is a good agreement between the MAPO values of the different sensors, which is validated by the coefficient of determinations (R^2) exceeding 0.7 for both plots. An equation for a linear trendline is included in the plots, which allows for a fair conversion between MAPO PCyl, MAPO Acc, and MAPO Mic. The other test fuels achieved similar correlation values. Some outlier cycles are marked in red, in which the MAPO knock intensities did not agree across sensors. A majority of cycles also showed very low MAPO knock intensities, which is not surprising since the D909 method required incipient knock conditions. Looking at the cyclic knock intensity distribution and defining a knock intensity threshold to determine between knocking and non-knocking conditions are targeted for the following discussions.

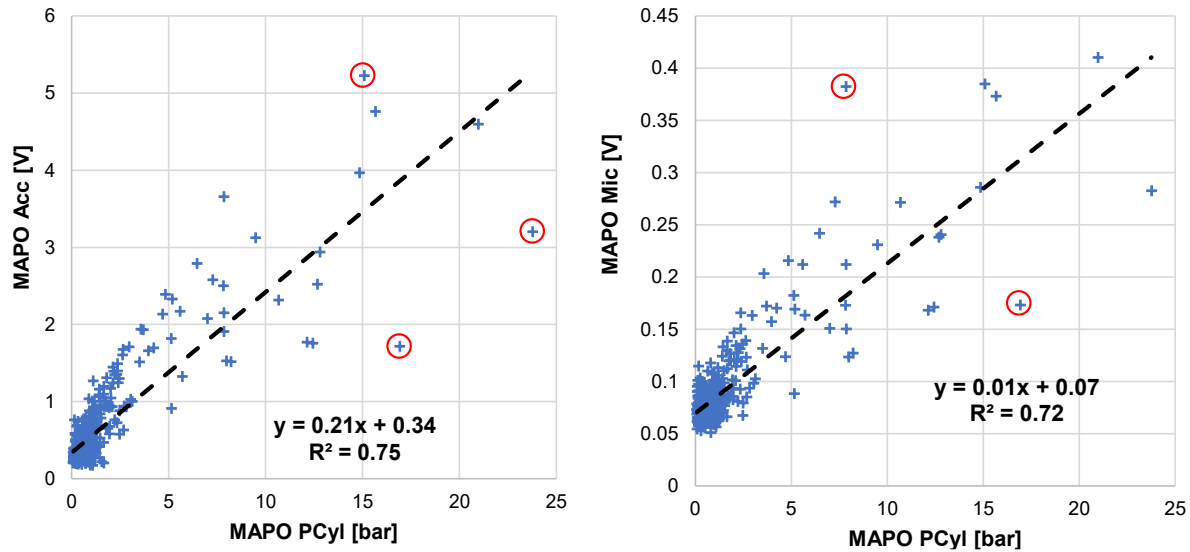


Figure 28. Correlation of MAPO Acc and MAPO Mic to MAPO PCyl for PRF100 operated at peak IMEP conditions and audible incipient knock. The plot includes 450 cycles, the coefficient of determination between the data points, and the respective linear trendline for the correlation of the sensors. Selected outliers are marked in red.

The ASTM D6424 method defines the Knock Number to evaluate the knock intensity of combustion cycles. Section 2.3.2. Knock Detection and Figure 12 (p.27) covered the details of the calculation method. Figure 29 shows a comparison of the calculated ASTM D6424 Knock Number to the cylinder pressure-based MAPO knock intensity for PRF100 operated at peak IMEP conditions and audible incipient knock conditions. The two types of data analysis rely on the same sensor but differ in their calculation procedure. This resulted in an excellent correlation ($R^2 = 0.96$) with minimal outliers. Subsequently, the Knock Number is also suitable for knock detection but is in its current development stage limited to signals from piezoelectric pressure sensors.

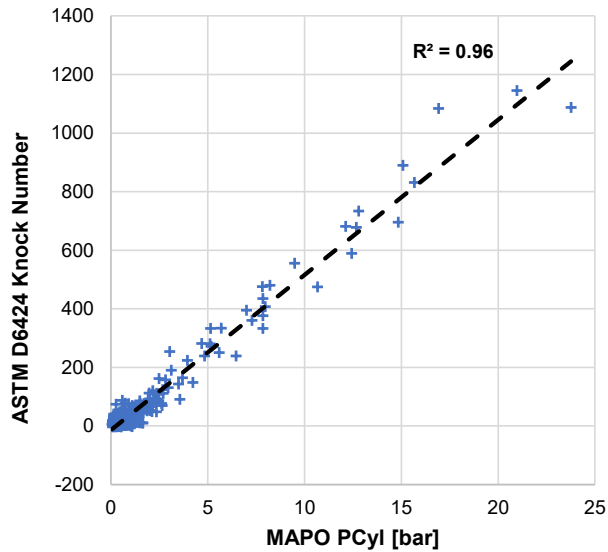


Figure 29. Correlation of the ASTM D6424 Knock Number knock intensity to the MAPO PCyl knock intensity for PRF100 operated at peak IMEP conditions and audible incipient knock.

The previous three figures showed that the knock intensity can significantly vary from minimal to high knock intensities from combustion cycle to combustion cycle. For determining a knock intensity threshold, it is important to understand the knock intensity distribution. Figure 30 shows three histograms that include a total of 450 cycles each and depict the number of cycles within a defined knock intensity range. These tests were performed with PRF100 at the audible knock limit and at peak IMEP conditions. All three knock detection instruments showed the majority of cycles with very low knock intensity. These cycles are likely non-knocking, which meets the incipient knock criteria of the D909 test method. There are also about 10% of the cycles that have significantly higher knock intensities. These select cycles are likely the cycles that create the audible pinging sound that the operator identifies as knock. The histograms show a non-normal distribution, so the averaged MAPO knock intensity cannot be used to represent the cases. Instead, a better approach is to define a fair knock intensity threshold to determine between knocking and non-knocking cycles. That would allow quantifying the relative number of knocking cycles.

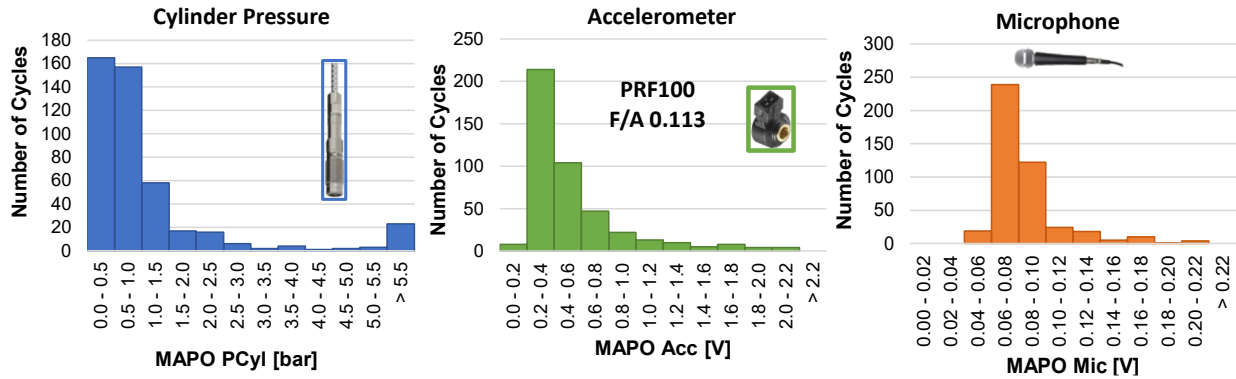


Figure 30. Cyclic distribution of MAPO PCyl, MAPO Acc, and MAPO Mic for PRF100 operated at peak IMEP conditions and audible incipient knock.

Section 5.1. Standard D909 Data Analysis discussed the performed fit for use test with iso+6ml TEL per US gal at a fixed intake pressure setpoint. The original purpose of the test is to baseline the engine and ensure that it operates within the specifications of D909. In addition, the test can also help to guide the determination between knocking and non-knocking cycles. Since this test is not conducted at incipient knock conditions, any calculated MAPO knock intensities would be signal noise rather than actual knock intensities. The high knock-resistance of the reference fuel in combination with the intake pressure setpoint creates non-knocking combustion cycles. The MAPO knock intensities for cylinder pressure (PCyl), accelerometer (Acc), and microphone (Mic) are calculated and their 450 cycle distribution is shown in Figure 31. The MAPO distribution was also found to follow a normal distribution. This ensured that all cycles of the fit for use case were at non-knocking conditions.

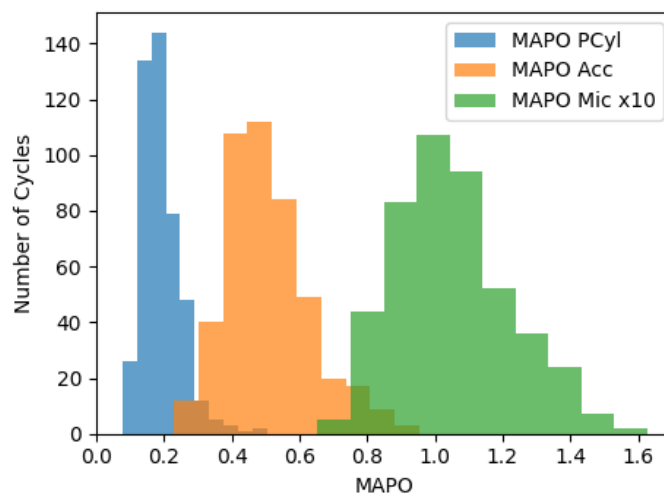


Figure 31. Histogram distribution of MAPO knock intensities for cylinder pressure (PCyl), accelerometer (Acc), and microphone (Mic) for non-knocking fit for use tests.

The highest non-knocking MAPO for the cylinder pressure, accelerometer, and microphone during a fit for use test are of special interest, since any cycles with similar or lower knock intensities than the threshold but tested under incipient knock conditions can be considered as non-knocking. The maximum non-knocking MAPO for cylinder pressure, accelerometer, and microphone were 0.51 bar, 0.95V, and 0.16V respectively. A MAPO PCyl threshold of 0.51 bar would classify the majority of cycles from *Figure 30* as knocking despite showing no significant pressure oscillations. A higher knock intensity threshold is targeted to ensure that only actual knocking cycles with noticeable pressure oscillations are considered. A common cylinder pressure-based knock intensity threshold used in automotive engine calibration is 1 bar per 1,000 rpm. Since the CFR F4 engine is operated at 1,800 rpm, a MAPO PCyl knock intensity threshold was selected at 1.8 bar. *Figure 28* established a linear trendline to convert the 1.8 bar MAPO PCyl knock intensity threshold to MAPO Acc (0.715V) and MAPO Mic (0.095V) thresholds. *Figure 32* shows the percentage of cycles exceeding this defined knock intensity threshold. Each data point consists of 450 consecutive cycles at steady-state operation. The data points across the three plots are at the same fuel-air ratios but the knock intensity was evaluated based on either the cylinder pressure transducer, the accelerometer, or the microphone. The data points and coloring in *Figure 32* are identical to the information presented in *Figure 16* (p.39) and *Figure 17* (p.39). The percentage of knocking cycles ranges from 0% to more than 80% of the cases knocking. The D909 test method states that not every cycle should be knocking, but some cycles must be knocking. The D909 test method does not provide a quantitative target in terms of the percentage of knocking cycles. A couple of observations stand out when comparing the data points across sensors or when comparing the knock information to the earlier IMEP data. Overall, most data points fall within the 10% to 50% of knocking cycles but little correlation between the effect of fuel-air ratio and the number of knocking cycles exists. This is likely due to the variation in operator perception of incipient knock. Generally, the percentage of knocking cycles aligns across sensors. The PRF85 (orange) had the highest percentage of knocking cycles at its leanest fuel-air ratio. It also had a higher-than-expected IMEP rating compared to the D909 framework in *Figure 16*, which suggests that the intermittent knock intensity criterion was exceeded in this case. Despite having a higher-than-expected IMEP, this specific point had the lowest overall IMEP of all cases, which can complicate the distinction between combustion and light-knocking cycles. PRF100 was tested at two differing conditions (*Figure 17*). First, PRF100 was tested based on audible incipient knock detection without regarding the D909 framework (green). Since this resulted in higher knock-limited IMEPs than the D909 framework allows, a repeat measurement directly at the IMEP targets (cyan) of the framework was performed. This second test resulted in 10% to 40% of knocking cases (based on all three sensors) at the four leanest fuel-air ratios

outside of the peak IMEP conditions. At the fuel-air ratio of peak IMEP and with an IMEP setpoint directly on the framework, 0% of the cycles were knocking. Subsequently, the D909 framework IMEP target is not knock-limited and would not meet the incipient knock requirement of the test method. This can potentially cause significant rating offsets should an operator select to perform audible knock-detection rather than following the framework for guidance, or anywhere in-between. Based on these observations, it is highly suggested that the D909 test method introduces a specific knock intensity target in terms of the percentage of knocking cycles beyond a defined knock intensity threshold.

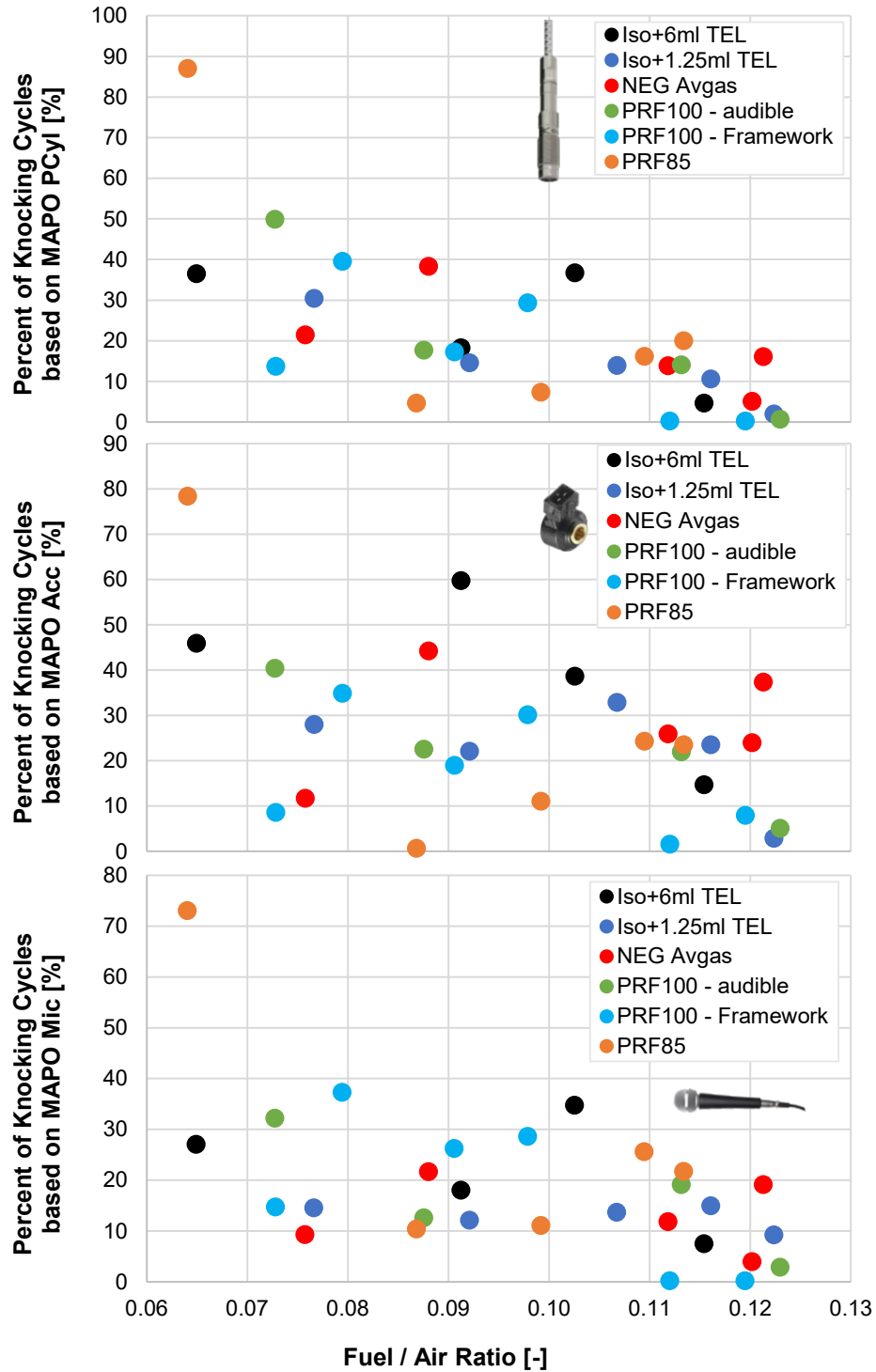


Figure 32. Percentage of knocking cycles for each sensor, fuel, and test condition.

All of the discussed and previously available knock detection systems for the D909 aviation method are said to have struggled with the reliable distinction between light knock and heavy non-knocking combustion. The ASTM D2699 RON test method describes the knockless knock phenomenon that can

occur for fuels with very high octane ratings such as benzene. As visualized in *Figure 10B* (p.24), knockless knock includes portions of the conventional deflagration combustion into the knock intensity calculation. This creates rating uncertainties due to over-estimated knock intensities. *Figure 33* shows a cylinder pressure trace (black) for PRF100 at peak IMEP ($F/A = 0.113$) under standard D909 rating conditions. The high-frequency pressure oscillations are seen to start after the initial peak cylinder pressure is surpassed. Previous knock detection systems could have counted this initial cylinder pressure peak into their knock intensity rating. *Section 2.3.2. Knock Detection* provided more detailed information about how the detonation meters work but generally, they are based on a lowpass-filtered trace which is included in orange in *Figure 33*. This is likely a significant contributor to the struggle to develop a reliable knock detection system for D909 applications.

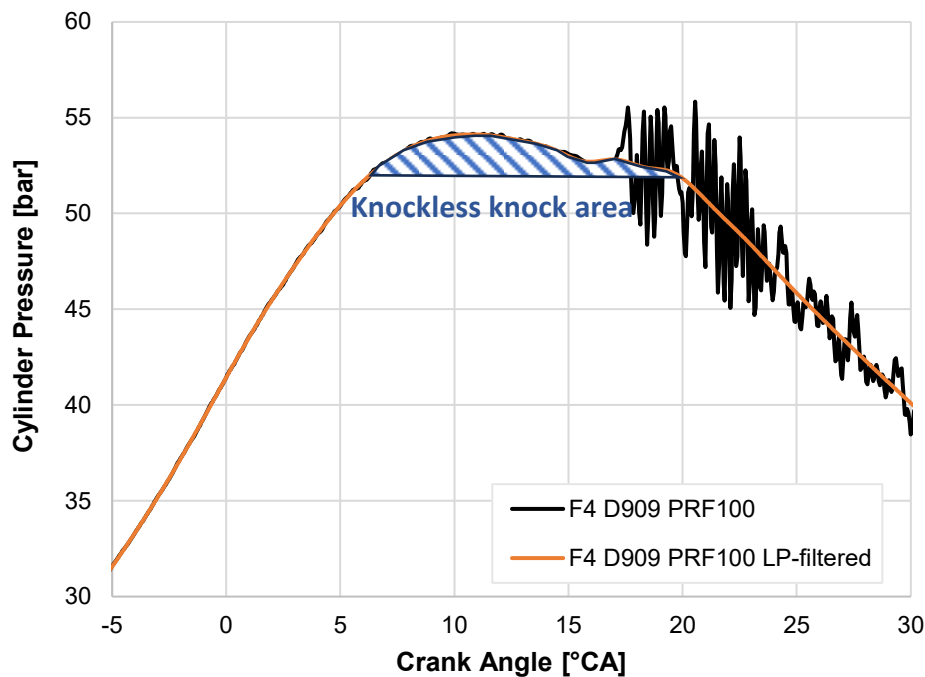


Figure 33. A cylinder pressure trace and a lowpass-filtered pressure trace for PRF100 operated at peak IMEP under standard D909 rating conditions with a marked knockless knock area.

This CFR F4 engine was equipped with state-of-the-art instrumentation to characterize the combustion and knocking conditions during standard D909 ratings. Knock detection methods based on high-frequency oscillations were able to evaluate the knock intensity of each cycle and determine between knocking and non-knocking conditions. The piezoelectric pressure transducer, accelerometer, and microphone were generally found to yield similar results. However, there are some considerations for their applicability for ratings in laboratories around the world. All sensors were synchronized to a crank angle encoder, which

is critical to limit the knock analysis to the combustion portion and neglect valve noise. While piezoelectric pressure transducers provide high-fidelity resolution and excellent natural frequencies for scientific combustion and knock analysis, they also require careful handling and calibration by highly trained operators. The accelerometer yielded similar results to the piezoelectric pressure transducer but requires significantly less investment, calibration, and care during its operation. The microphone also yielded similar results, but care was taken to limit ambient noise from surrounding engines during these specific D909 tests. Overall, the accelerometer is the best compromise between data resolution, handling, required calibration, and financial investment.

6. Thermodynamic Modeling of D909 Test Conditions

The added instrumentation on the CFR F4 engine allowed for a cylinder pressure-based characterization of combustion and knocking conditions. A fuel's autoignition is a requirement for knocking combustion. Autoignition depends on the time that the fuel-air mixture spends at a given pressure-temperature condition. The pressure and time aspects are known from cylinder pressure and encoder measurements. Measurement of in-cylinder crank angle-resolved temperature is an ongoing challenge in engine combustion research. Instead of temperature measurements, the cylinder pressure-temperature conditions can be modeled. This will enable a better understanding of the cylinder conditions leading up to spark timing and allow for a comparison to actual aviation piston engines. This section will also compare the pressure-temperature conditions of the D909 supercharge method to those of standard RON and MON conditions.

A widely used commercial modeling software from Gamma Technologies was used for this study. The GT-Power software allows for a three-pressure analysis (TPA) model to estimate cylinder pressure-temperature conditions based on crank angle-resolved measurements of the intake, cylinder, and exhaust pressures. The intake and exhaust port temperatures were also measured and used as input to the GT model. Having defined boundary conditions in the intake and exhaust ports removes the requirement to model the entire intake and exhaust systems, which reduces simulation uncertainties. Furthermore, the measured cylinder pressure trace is used for a heat release analysis by GT-Power, which is then applied in the model for the simulated pressure trace. This removes the need to calibrate a Wiebe heat release model, which is likely going to struggle with the unique heat release rate for knocking combustion. Previous studies at Argonne National Laboratory have already developed GT-Power TPA models for the CFR F1 (RON), CFR F2 (MON), supercharged knocking SI, and homogenous charge compression ignition conditions [Choi, 2018; Pulpeiro, 2019]. The reader is referred to two previous publications, which explain in detail the development efforts and selected models. This report will summarize the most important models that were used in the TPA model. A detailed overview of the required modifications of the model for the CFR F4 engine is also provided in this report.

The overall GT-Power TPA model for the CFR F4 engine is shown in *Figure 34*. The developed CFR engine TPA model uses a 3D-scanned CFR cylinder head for accurate geometries in the finite element structure. The heat transfer was calculated by the WoschniGT model for the geometry of the finite element cylinder head. In addition, specific heat transfer multipliers were added to scale the heat transfer during the model

calibration to account for knocking combustion. This is required since knocking combustion can increase the heat transfer as the high-frequency pressure oscillations penetrate the boundary layer of the combustion chamber surfaces. An integrated design optimizer was used to find the optimal heat transfer multiplier during combustion to minimize offsets between the simulated and measured cylinder pressure. Also, GT-Power is widely used by the automotive industry and is subsequently tailored to modern engine designs. Meanwhile, the CFR engine cylinder head geometry was initially designed in the 1930s, which can impact heat transfer due to the selected materials and geometries.

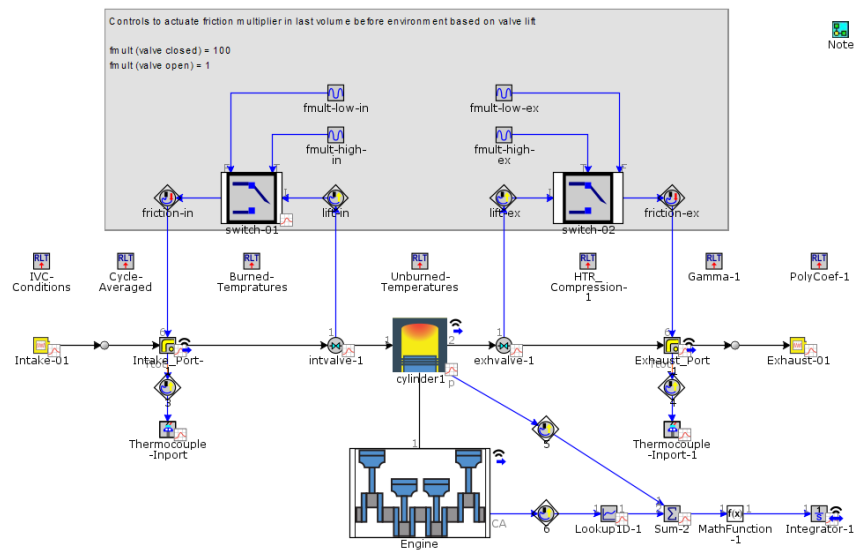


Figure 34. Overview of the GT-Power TPA model for the CFR F4 engine.

The starting point for the CFR F4 engine model was the previously developed CFR F1 (RON) model described in two previous publications [Choi, 2018; Pulpeiro, 2019]. Several modifications were made to customize the TPA model for CFR F4 conditions. First, the overall boundary conditions were updated as specified by the D909 test method and as measured by pressure and temperature sensors mounted on the engine. Next, the geometry differences and respective materials were updated. The piston material was changed from cast iron to an aluminum alloy. The compression ratio was set to 7:1 in accordance with the D909 method. The intake and exhaust valve material and geometry were updated, along with their respective valve lift profiles provided by CFR Engines Inc. Professor DelVescovo from Oakland University provided flow bench measurements for the F4's unique intake and exhaust valves, which were incorporated in the CFR F4 model. While a wideband lambda sensor was installed on the CFR F4, its readings were unreliable due to the excessively rich fuel-air mixture and the usage of leaded fuels. GT-Power uses the measured fuel and air mass flow to estimate the mixture composition. A stoichiometric

air-to-fuel ratio was calculated based on the known composition of PRFs. The tetraethyl lead was omitted for the PRFs in GT-Power since the very small concentration does not impact the polytropic coefficients. The increased knock resistance of the fuel due to TEL is still considered since GT-Power uses a measured heat release rate for its simulation. The NEG Avgas is a mixture of numerous components. GT-Power requires the fuel composition to estimate the polytropic coefficients. Fuels within a given chemical family have similar physical properties, which allows for one representative compound for one chemical family. This study had access to a hydrocarbon analysis that specified the concentrations of select chemical families. The chemical families were modeled with iso-octane to represent paraffins, toluene to represent aromatics, and diisobutylene to represent olefins. GT-power also needs to simulate the exhaust gas composition to calculate polytropic coefficients and to estimate the combustion efficiency. An emissions bench to measure exhaust gas composition was not available for the F4 engine measurements. However, emissions data for extended air-fuel ratio sweeps during standard RON ratings with PRF100 were available at Argonne National Laboratory. *Figure 35* shows the total hydrocarbon (THC), nitric oxide (NO), carbon monoxide (CO), and oxygen (O₂) concentrations based on lambda. The CFR F4 engine operates at lambda values between 0.5 and 1.0, which requires extrapolation outside of the available measured emissions data. However, the linear trendlines at rich conditions ($\lambda < 1$) for CO and THC suggest that extrapolations are acceptable. The exhaust oxygen concentration and NO concentrations asymptote towards zero for very rich conditions.

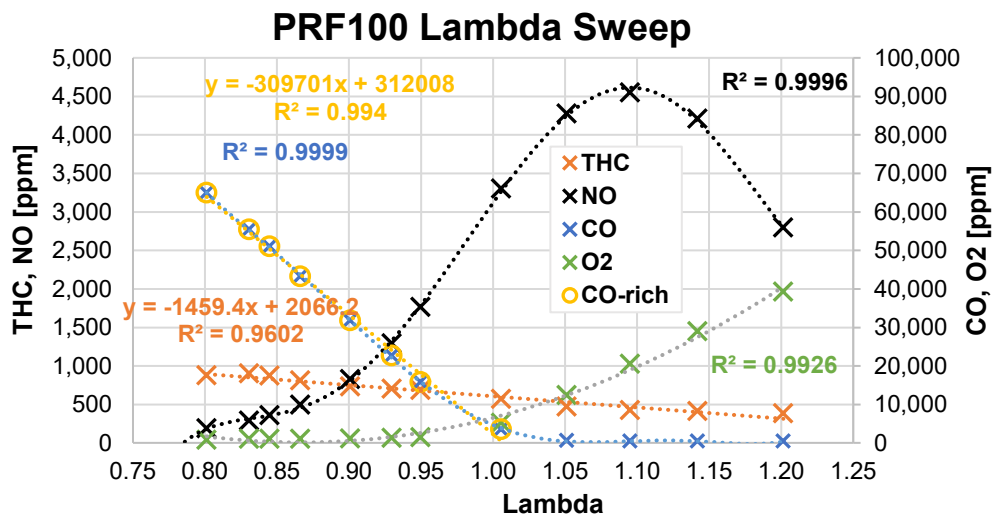


Figure 35. Exhaust emissions measurements for standard RON operation of PRF100 at Argonne National Laboratory.

The GT-Power TPA model requires a measured cylinder pressure trace as an input parameter. For each steady-state condition, 450 consecutive cycles were measured. *Figure 36* shows 450 cylinder pressure traces for PRF100 tested at peak IMEP conditions. An ensemble-averaged pressure trace (black) is overlaid. However, an average pressure trace is not representative of conditions that include knocking cycles since the high-frequency pressure oscillations create destructive interference, which averages out the specific knock information. This is also noticeable in the averaged trace (black) in *Figure 24* (p.46). Subsequently, a representative cylinder pressure trace needed to be selected. Some combustion and knocking characteristics do not follow normal distributions so skewed data need to be considered. Pulpeiro et al. established a pathway to select the most representative cycle, which takes numerous combustion and knocking characteristics into account and is suitable for skewed data [Pulpeiro, 2021]. This selection process for the most representative cycles was followed and the three most representative cycles (MRC) are depicted in *Figure 36*. The second most representative cycle (orange) closely follows the average pressure trace and was selected as the representative cycle for the GT-Power model.

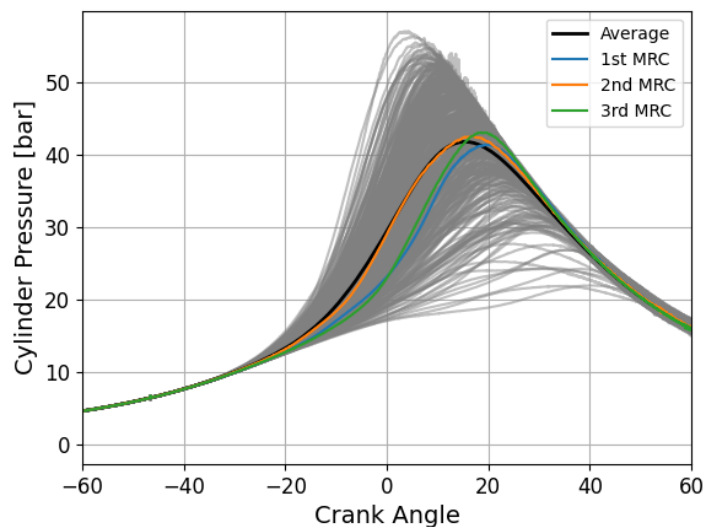


Figure 36. Cylinder pressure trace of 450 consecutive cycles for PRF100 operated at peak IMEP conditions. The three most representative cycles (MRC) are overlaid, along with an averaged pressure trace for reference.

The final TPA model provided a simulated pressure trace that was compared to the measured most representative cylinder pressure trace in *Figure 37* for PRF100 at peak IMEP conditions. Ideally, the simulated pressure trace closely matches the MRC so that the simulated pressure-temperature conditions are accurate. Areas of specific interest are the gas exchange (cf. bottom plot of *Figure 37*) and the compression stroke up to spark timing (cf. top plot of *Figure 37*). While GT-Power uses a two-zone model for temperature estimation after spark timing, the uncertainties generally increase during the combustion

portion of the cycle. Subsequently, the TPA model is only used to estimate pressure-temperature conditions leading up to spark timing. GT-Power has numerous parameters that allow for calibration of the model to align the simulated with the measured pressure trace. For the final calibrated model, the maximum cylinder pressure offset at spark timing was 3% and the simulated IMEP was within 9% of the measured cycle.

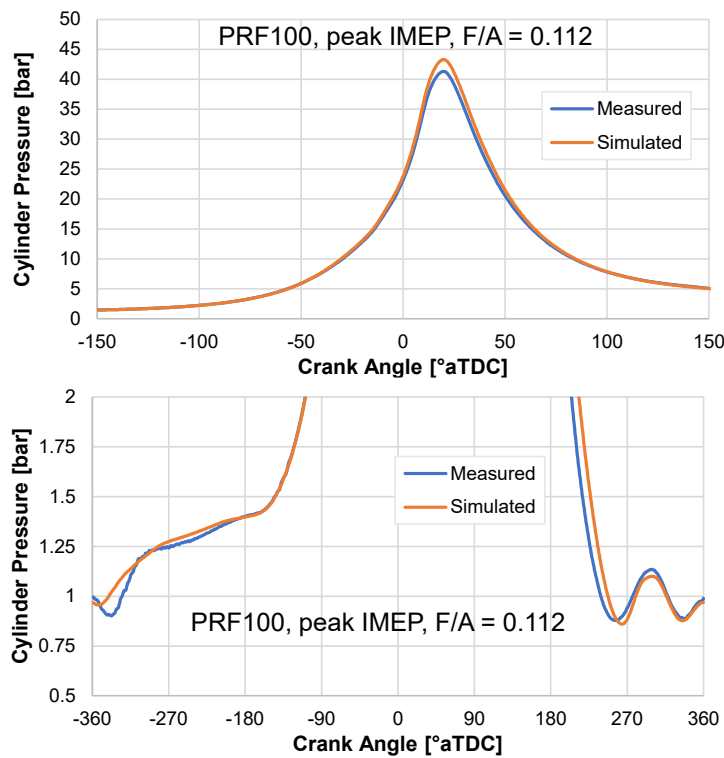


Figure 37. Comparison of the simulated cylinder pressure trace during compression, combustion, and expansion (top plot) and during gas exchange (bottom plot).

The resulting pressure-temperature trajectories during compression for all test fuels at peak IMEP conditions are shown in Figure 38. The pressure-temperature trajectories start with intake valve closing (IVC) and continue until spark timing. Therefore, the entire polytropic compression stroke is depicted in the figure. Fuels with increased knock resistance allowed for a higher knock-limited IMEP in Figure 16 (p.38), which in turn had a higher intake pressure setpoint. Subsequently, PRF85 showed the lowest starting point of cylinder pressure, and iso+6ml had the highest, respectively. All tested fuels under D909 conditions had an almost identical starting temperature for the P-T trajectories since the mixture temperature was almost identical across the fuels due to a similar heat of vaporization. The pressure-temperature trajectories for iso+1.25 and NEG Avgas are almost identical since their knock resistance and the resulting test conditions were closely aligned. In addition to the fuels tested under D909 test

conditions, the P-T trajectories for standard RON and MON are also shown in *Figure 38*. The motor octane number test is operated at a much-increased mixture air temperature, which shifted its P-T trajectory towards higher in-cylinder temperatures. The P-T trajectory for the standard RON test closely matches that of PRF100 tested under D909 test conditions. Subsequently, the CFR F1 configuration likely has the potential to recreate ratings similar to the D909 method up to PRF100. A previous study by the authors developed a supercharged version of the standard RON test to rate the knock resistance of automotive gasoline at conditions more closely aligned with modern turbocharged engines [Hoth, 2023]. A compressed air intake manifold was developed for the CFR F1 engine and the Supercharged Octane Number (SON) was tested at 1.5 bar intake pressure. The P-T trajectory of that test is also included in *Figure 38* and closely aligns with those of NEG Avgas and Iso+1.25ml. Subsequently, the CFR F1 engine with a compressed air intake manifold could be able to reproduce cylinder conditions similar to D909 ratings up to typical performance numbers of aviation gasoline. The CFR F1 engine at Argonne is currently undergoing an upgrade to allow up to 3.0 bar intake pressure, which will be able to exceed the P-T trajectory of iso+6ml. Therefore, supercharging a F1/F2 octane rating engine could a potential path forward to upgrading the D909 test method to be operated on this widely available test platform.

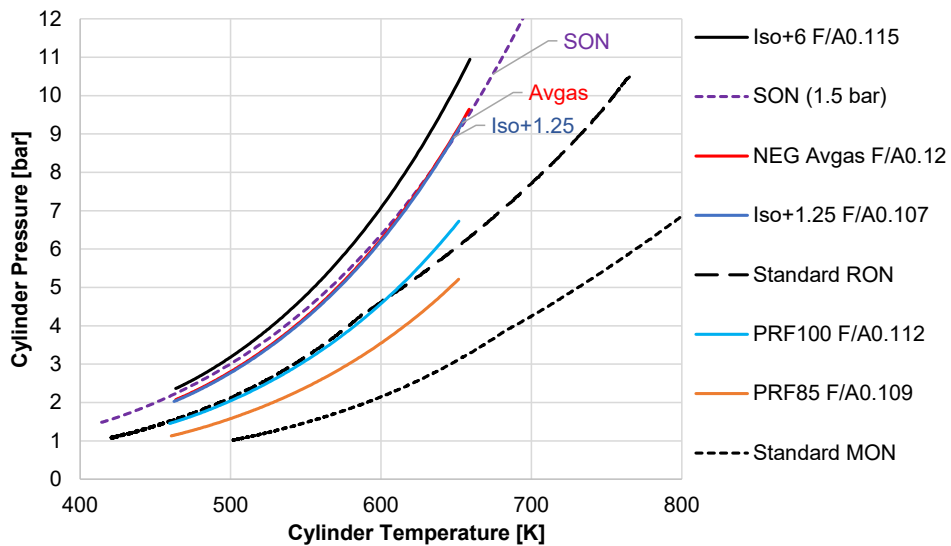


Figure 38. Pressure-Temperature trajectories for all tested fuels at peak IMEP conditions. In addition, the P-T trajectories for standard RON and MON are overlaid, along with a P-T trajectory for a RON test performed at 1.5 bar intake pressure (SON).

The D909 test method requires fuel-air ratio sweeps to be performed to validate the engine’s performance against the available framework. The fuel’s resistance to knock changes with the fuel-air ratio, which results in changes to the intake manifold pressure. *Figure 39* depicts the P-T trajectories for

six fuel-air ratios for PRF100 tested under standard D909 test conditions. The intake pressure effect on the starting point of the P-T trajectory is closely noticeable. Furthermore, the starting temperature of the P-T trajectory also shifts with fuel-air ratio. As more fuel is injected into the manifold, more evaporative cooling occurs which reduces the mixture temperature and the temperature at IVC. Furthermore, the heat capacity of the mixture also changes, which can impact the temperature development until intake valve closing.

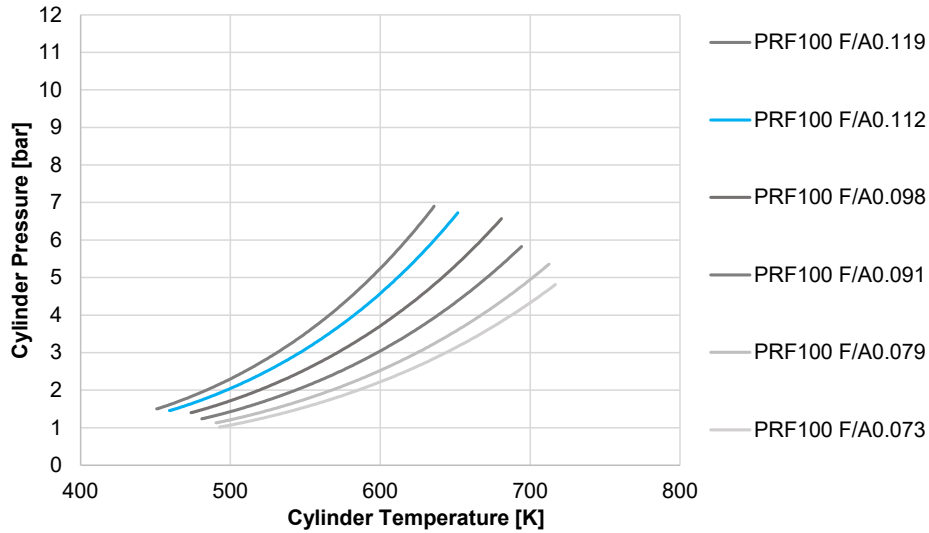


Figure 39. Pressure-Temperature trajectories for PRF100 for a fuel-air ratio sweep. The blue line identifies the peak IMEP condition for PRF100.

The shown P-T trajectories for the D909 test method allow for a better understanding of the thermodynamic conditions in the combustion chamber leading up to spark timing. Fuels with increased knock resistance allowed for significantly higher pressure-temperature conditions before reaching their knock limit. The CFR F1 RON configuration can replicate the conditions of the D909 test method up to PRF100. When using a compressed air intake manifold, the rating conditions up to and beyond NEG Avgas can be replicated by a modified supercharged version of the CFR F1 engine. Testing the reactivity of Avgas in a more widely distributed CFR F1 engine is a suggested item for future work. A more detailed discussion and additional future work possibilities are discussed in *Chapter 8. Future Work*.

7. Summary

This study analyzed the combustion and knocking characteristics of the D909 aviation supercharge rating. A literature study reviewed development efforts for the D909 test method and respective knock detection devices, along with a definition of knocking combustion. The experimental study was conducted at CFR Engines Inc., which upgraded a standard CFR F4 engine with state-of-the-art combustion research instrumentation. The test fuels included PRF85, PRF100, PRF100 +1.25 ml TEL per gal, PRF100 + 6 ml TEL per gal, and NEG Avgas, covering the entire range of thermodynamic conditions of the D909 test method. The first set of engine tests was performed at audible incipient knock detection by the operator without using the D909 framework to prevent implicit bias on the perceived knock limit. The resulting IMEP values exceeded those defined by the D909 framework, despite the F4 engine passing the non-knocking Fit for Use test. A second test with PRF100 followed the D909 framework precisely while disregarding the perceived knock intensity so that a knock intensity characterization was performed on the framework itself as well.

The measured cylinder pressure traces were used to characterize general combustion properties such as combustion phasing and IMEP, which revealed an offset between the dynamometer load cell-based F4 IMEP measurement and the cylinder pressure-based IMEP. The IMEP measurement offset scaled with engine load, suggesting an artificial impact of intake pressure on the measured friction mean effective pressure. The cyclic pressure-based IMEP analysis revealed misfire and partial burn cycles at the richest fuel-air ratio setpoints of a standard D909 test.

The CFR F4 engine was equipped with a piezoelectric pressure transducer, an automotive accelerometer-based knock sensor, and a microphone next to the operator. This allowed capturing of the signal chain from knocking combustion within the combustion chamber, via the vibrations of the cylinder head, to the air pressure waves that the operator would hear. The knock intensity of all three sensors was quantified by the maximum amplitude of pressure oscillations (MAPO), and the relative correlation across sensors exceeded $R^2 > 0.7$. However, a crank angle delay was noticed since the pressure waves needed to travel through and transfer between different mediums. The ASTM 6424 Knock Number for aviation engines showed an excellent correlation with the cylinder pressure-based MAPO knock intensity. The MAPO knock intensity for all three sensors showed skewed, non-normal distributions due to a large number of non-knocking conditions, which renders the average knock intensity invalid. Subsequently, a knock intensity threshold was defined to determine between knocking and non-knocking cycles. For the 450 recorded

consecutive cycles per data point, between 0% and 90% of the cycles were knocking, but it greatly varied between cases for audible incipient knock detection. The majority of cases showed 10% to 50% of knocking cycles, thus meeting the D909 incipient knock criteria. PRF85 experienced the highest number of knocking cycles at the lowest overall IMEP setpoint, suggesting that incipient knock detection at low load conditions can be challenging. Notably, PRF100 operated directly at the peak IMEP target of the D909 threshold had 0% of its cycles knocking, therefore not meeting the incipient knock criteria set by the D909 test method despite the engine meeting the non-knocking fit for use criteria. A defined knock intensity threshold and a targeted percentage of knocking cycles that exceed said threshold would greatly improve the apparent uncertainty of the current test method. The piezoelectric pressure sensor is ideal for scientific combustion and knock research but requires higher financial investment, trained operators, and careful calibration on a regular basis. The microphone offered similar results but is sensitive to the mounting orientation and can be disturbed by surrounding noise, especially when operating multiple engines in close proximity. The accelerometer also showed similar knock intensity results, but is not impacted by surrounding engines, and is readily available from commercial automotive applications, which makes it a promising candidate for knock detection of a future D909 test method. Based on the cylinder pressure measurements in this study, earlier knock detection systems likely suffered from knockless knock measurements.

Simulations of thermodynamic in-cylinder pressure-temperature conditions of standard D909 tests were performed with GT-Power. Fuels with increased knock resistance allowed for higher P-T conditions resulting in higher knock-limited IMEP values. The standard RON and MON rating engine can recreate similar thermodynamic cylinder conditions of PRF85 up to PRF100. A compressed air intake manifold, like the one available at Argonne's CFR engine, can create similar thermodynamic conditions to that of Avgas and Iso+1.25 TEL. Replicating thermodynamic cylinder conditions representative of D909 testing of iso+6 TEL likely requires intake pressures of up to 2.0 bar on the F1 CFR engine.

8. Future Work

This study provided the first comprehensive analysis of combustion, knocking, and thermodynamic conditions of the D909 test method with a host of modern engine combustion research instruments and methods. Knocking combustion creates high-frequency pressure oscillations that are audible to the operator. The piezoelectric pressure sensor enabled scientific analysis of knock intensity amplitudes, but a frequency analysis was outside the scope of this work. Recommended knock intensity characterizations are Fast-Fourier Transform (FFT) analysis for respective knock frequencies and subsequent knock spectral energy calculations to determine the intensity of specific knock frequencies, which can help to correlate to audible knock.

The D909 test method requires CFR F4 operation at knock-limited IMEP, which also has to align with the specified framework. This study revealed that audible knock detection without consideration of the framework can exceed knock-limited IMEP targets. Furthermore, when operating directly at the IMEP specified by the framework, it is possible that 0% of cycles could be knocking at peak IMEP conditions for PRF100. Follow-up work could dive deeper into the Fit for Use determination relative to the framework, and define a knock intensity threshold to require a specified percentage of cycles that exceed that threshold. This updated method would guarantee a specific and repeatable knock limit for D909 rating conditions and reevaluate the currently available framework.

The thermodynamic simulations of the D909 rating conditions showed that the in-cylinder pressure-temperature conditions can be replicated by a CFR engine in RON configuration up to PRF100. A compressed air intake system upgrade for a CFR F1 engine would further allow replication of cylinder thermodynamic conditions of the full D909 range. Argonne's CFR engine already includes a compressed air intake system capable of greater than 2.0 bar intake pressure. Such a similar setup could be used in future work to rate the performance number of aviation gasoline in an upgraded CFR F1 engine and compare it to conventional F4 ratings. Other operational parameters such as coolant temperature and engine speed need consideration for replicating D909 rating conditions in a modified RON rating engine.

This study was limited to four reference fuels and one commercial aviation gasoline. These fuels allowed to capture the entire range of thermodynamic conditions of the D909 test method but did not include unleaded aviation gasoline variants. Unleaded aviation gasolines likely include non-paraffinic compounds, which will shift their stoichiometric air-to-fuel ratio and result in a shifted IMEP curve relative to the

framework. The D909 method could be improved by switching to an equivalence ratio-based scaling that would enable an improved rating of highly aromatic or oxygenated aviation gasoline. Binary blends of iso-octane with ETBE or aromatic amines and a fixed performance number would enable research of fuel-specific impacts on the D909 test method.

The D909 supercharge aviation test method rates the knock resistance of aviation gasoline during peak load conditions of aviation combustion engines. A detailed comparison of temporal and thermodynamic conditions between the D909 conditions and commercial aviation engines is suggested. This can also be combined with unleaded aviation gasolines that potentially impact the stoichiometric air-to-fuel ratio.

Acknowledgments

The authors would like to thank the Coordinating Research Council (CRC) Aviation task group for funding this AV-28-19 project and providing project guidance. Special thanks to CFR Engines Inc., who upgraded their CFR F4 engine with state-of-the-art combustion research instruments, performed all experimental test runs for this study and provided the data to CRC. The authors also acknowledge the work of Professor Dan DeVescovo from Oakland University for providing flow bench measurements for the CFR F4 intake and exhaust valves.

Argonne is a U.S. Department of Energy laboratory managed by UChicago Argonne, LLC under contract DE-AC02-06CH11357.

References

Reference Name	Reference Details
ASTM D2699	ASTM International, D2699-23A "Standard Test Method for Research Octane Number of Spark-Ignition Engine Fuel". West Conshohocken, PA; ASTM International, 2023.
ASTM D2700	ASTM International, D2700-23A "Standard Test Method for Motor Octane Number of Spark-Ignition Engine Fuel". West Conshohocken, PA; ASTM International, 2023.
ASTM D6424	ASTM International, "Standard Practice for Octane Rating Naturally Aspirated Spark Ignition Aircraft Engines", West Conshohocken, PA, 2019

ASTM D909-1995	ASTM International, D909-95 "Standard Test Method for Supercharge Rating of Spark-Ignition Aviation Gasoline". West Conshohocken, PA; ASTM International, 1995.
ASTM D909-2022	ASTM International, D909-22 "Standard Test Method for Supercharge Rating of Spark-Ignition Aviation Gasoline". West Conshohocken, PA; ASTM International, 2022.
ASTM D910, 2021	ASTM International, D910-21 "Standard Specification for Leaded Aviation Gasolines". West Conshohocken, PA; ASTM International, 2021.
ASTM Manual, 1973	ASTM International, ASTM Manual for Rating Motor, Diesel, and Aviation Fuels 1973-74. Philadelphia; American Society for Testing and Materials, 1973.
ASTM Minutes, 1954	ASTM Minutes of D02 Meeting on October 4, 1954.
ASTM Minutes, 1955	ASTM Minutes of D02 Meeting on June 29, 1955. Appendix A.
ASTM RR:D02-1986	Jones, J., "Report of Supercharge Method Seminar Task Force to ASTM Subcommittee D02.01 on Combustion Characteristics", June 29, 1986.
ASTM RR:D02-69, 1970	ASTM research report RR:D02-69 "Aviation Gasoline Antiknock Quantity by ASTM Methods D614 and D357", 1970.
ATSDR, 2019	Agency for Toxic Substances and Disease Registry (ATSDR). 2019. Toxicological profile for Lead. (Draft for Public Comment). Atlanta, GA: U.S. Department of Health and Human Services, Public Health Service.
Bartholomew, 1961	Bartholomew, E., "New Knock-Testing Methods Needed to Match Engine and Fuel Progress," SAE Technical Paper 610200, 1961, https://doi.org/10.4271/610200
Baxter, 1956	Waukesha Motor Company, Baxter, I., Personal letter from Mr. Baxter to Socony Mobil Oil Company. August 7, 1956.
Bogin, 2016	Bogin, G., Luecke, J., Ratcliff, M, et al., "Effects of iso-octane/ethanol blend ratios on the observance of negative temperature coefficient behavior within the Ignition Quality Tester", Fuel, Volume 186, 2016, p.82 - 90. https://doi.org/10.1016/j.fuel.2016.08.021
Boyd, 1946	Boyd, T., "The Bouncing-Pin Indicator Is 25 Years Old," SAE Technical Paper 460135, 1946, https://doi.org/10.4271/460135 .
Cessna 152	Cessna, "Information Manual Model 152", Pilot's Operating Handbook 1980.
CFR Inc., 2015	CFR Engines Inc., "CFR F1/F2 Octane Rating Unit Operation & Maintenance Manual", 4th Edition, 2015.

CFR Inc., 2015A	CFR Engines Inc., "CFR F4 Aviation Gasoline Rating Unit Operation & Maintenance Manual", 3rd Edition, 2015.
Choi, 2018	Choi, S., Kolodziej, C., Hoth, A., and Wallner, T., "Development and Validation of a Three Pressure Analysis (TPA) GT-Power Model of the CFR F1/F2 Engine for Estimating Cylinder Conditions," SAE Technical Paper 2018-01-0848, 2018, https://doi.org/10.4271/2018-01-0848 .
CRC, 1945	Coordinating Research Council, "Report on the Knock Intensity", Report 18, New York, 1945
Dernotte, 2014	Dernotte, J., Dec, J., and Ji, C., "Investigation of the Sources of Combustion Noise in HCCI Engines," SAE Int. J. Engines 7(2):730-761, 2014, https://doi.org/10.4271/2014-01-1272 .
Draper, 1934	Draper, C.S., "The Physical Effects of Detonation in a Closed Cylindrical Chamber", NACA Report 493, 1934.
Draper, 1938	Draper, C.S., "Pressure Waves Accompanying Detonation in the Internal Combustion Engine," Journal of the Aeronautical Sciences, Vol. 5, 1938.
Draper, 1944	Draper, C.S., Taylor E., Lancor, J., et al., "Development of a Detonation Detector Suitable for Use in Flight", National Advisory Committee for Aeronautics, 1944. Reprint of AQR, November 1939.
EIA 2024	U.S Energy Information Administration, Monthly Energy Review, March 29, 2022, with data added from January 2024 Monthly Energy Review
EPA, 1996	EPA. 1996a. Prohibition on gasoline containing lead or lead additives for highway use. U.S. Environmental Protection Agency. Fed Register 61(23):3832.
FAA EAGLE	Federal Aviation Administration, "Eliminate Aviation Gasoline Lead emissions (EAGLE)", https://www.faa.gov/unleaded , accessed Feb. 13, 2024.
Gibbs, 1990	Gibbs, L. (1990). Gasoline additives—when and why. SAE Trans. 99, 618–638. doi:10.4271/902104
Gulf Oil Corporation, 1955	Gulf Oil Corporation, "Phillips 103-A Knockmeter", Personal letter from Mr. French to Mr. Snell and Members of the Supercharge Method Study Group. February 4, 1955
Hoffman, 1961	Hoffman, R., "A New Technique for Determining the Knocking Resistance of Fuels," SAE Technical Paper 610202, 1961, https://doi.org/10.4271/610202 .

Hoth, 2023	Hoth, A., Kolodziej, C., Waqas, M., Szybist, J., Miers, S., "Development of a Supercharged Octane Number and a Supercharged Octane Index," SAE Technical Paper 2023-01-0251, 2023, https://doi.org/10.4271/2023-01-0251 .
Hoth, 2024	Hoth A., "Investigation of Operational Parameter Differences Between the Standard RON Test Method and Knock-Limited Modern Spark-Ignition Engine Operation", Dissertation, Michigan Technological University, 2024.
Kitman, 2000	Kitman, J.L. (2000). The secret history of lead. Nation N.Y. 270, 11–11.
Kumar, 2018	Kumar, T., Mohsin, R., Ghafir, M., et al., "Concerns over use of leaded aviation gasoline (avgas) fuel", Chemical Engineering Transactions, 2018, 63, 181-186 DOI:10.3303/CET1863031.
Kumar, 2019	Kumar, T., Mohsin, R., Majid, Z., Ghafir, M. et al., "Response Surface Methodology (RSM) in Optimization of Performance and Exhaust Emissions of RON 97, RON 98, and RON 100 (Motor Gasoline) and AVGAS 100LL (Aviation Gasoline) in Lycoming O-320 Engine," SAE Int. J. Engines 12(4):427-454, 2019, doi:10.4271/03-12-04-0029.
Kumar, 2020	Kumar, T., Mohsin, R., Majid, Z., et al., "Experimental study of the anti-knock efficiency of high-octane fuels in park-ignited aircraft engine using response surface methodology", Applied energy, Volume 259, February 2020. doi:10.1016/j.apenergy.2019.114150
Leake, 1926	Leake, J.P., Kolb, L., Howell, W.H., Chesley, A.J., Edsall, D.L., Hunt, R., et al. (1926). The Use of Tetraethyl Lead Gasoline in its Relation to Public Health. Washington, DC
Lee, 2008	Lee, J., "The Detonation Phenomenon", Chapter 8 - Deflagration-to-Detonation Transition, pp. 250 - 296, Cambridge University Press, Print publication year: 2008. https://www.cambridge.org/core/books/abs/detonation-phenomenon/deflagrationtodetonation-transition/FB9A50CF3318A8D5B82C8AAF857E8FAB
MacCoull, 1936	MacCoull, N. and Stanton, G., "The Measurement of Engine Knock by Electro-Acoustic Instruments," SAE Technical Paper 360104, 1936, https://doi.org/10.4271/360104 .
Midgley, 1920	Midgley, T., "High-Speed Indicators," SAE Technical Paper 200011, 1920, https://doi.org/10.4271/200011 .

Midgley, 1922	Midgley, T. and Boyd, T., "METHODS OF MEASURING DETONATION IN ENGINES," SAE Technical Paper 220004, 1922, https://doi.org/10.4271/220004 .
Minjares, 2019	Minjares, R., Walsh, M., "Methylcyclopentadienyl Manganese Tricarbonyl (MMT): A Science and Policy Review", The international council on clean transportation, January 2019
Mittal, 2009	Mittal, V., "A study of the Physics and Chemistry of Knock in Modern SI Engines and Their Relationship to the Octane Tests", Dissertation, Massachusetts Institute of Technology, 2009.
Neddleman, 1998	Needleman, H.L.(1998). Child hood lead poisoning: the promise and abandonment of primary prevention. Am.J. Public Health 88, 1871–1877. doi:10.2105/AJPH.88.12.1871
Phillips66, 1956	Phillips 66 Instruments, "The Electronic Gating Knockmeter, Operating and Maintenance Instructions. Bartlesville, 1956.
Price, 2019	Price, H., "Fact Sheet – Leaded Aviation Fuel and the Environment", Federal Aviation Administration (FAA), November, 2019. https://www.faa.gov/news/fact_sheets/news_story.cfm?newsId=14754 .
Pulpeiro, 2019	Pulpeiro Gonzalez, J., Waqas, M., Kolodziej, C., DeIVescovo, D. et al., "Improvements to a CFR Engine Three Pressure Analysis GT-Power Model for HCCI and SI Conditions," SAE Technical Paper 2019-32-0608, 2020.
Pulpeiro, 2019A	Pulpeiro Gonzalez, J., Waqas, M., Kolodziej, C., DeIVescovo, D. et al., "Improvements to a CFR Engine Three Pressure Analysis GT-Power Model for HCCI and SI Conditions," SAE Technical Paper 2019-32-0608, 2020.
Pulpeiro, 2021	Pulpeiro, J., Hall, C., Kolodziej, C., "Determination of a most representative cycle from cylinder pressure ensembles via statistical method using distribution skewness", International Journal of Engine Research. 2021. Vol, 24(2) p.720-737.
Robert, 1983	Robert, J.C.(1983). Ethyl: A History of the Corporation and the People Who Made It. Charlottesville, VA: University Press of Virginia, 448.
Rockstroh, 2018	Rockstroh, T., Kolodziej, C., Jespersen, M., Goldsborough, S. et al., "Insights into Engine Knock: Comparison of Knock Metrics across Ranges of Intake Temperature and Pressure in the CFR Engine," SAE Int. J. Fuels Lubr. 11(4):545-561, 2018, https://doi.org/10.4271/2018-01-0210 .
Rockstroh, 2018	Rockstroh, T., Kolodziej, C., Jespersen, M., Goldsborough, S. et al., "Insights into Engine Knock: Comparison of Knock Metrics across Ranges of Intake Temperature

	and Pressure in the CFR Engine," SAE Int. J. Fuels Lubr. 11(4):545-561, 2018, https://doi.org/10.4271/2018-01-0210 .
Siegel, 1954	Siegel B., "Phillips 103-A Detonation Meter", Personal letter from Mr. Siegel to Mr. Snell and Members of the Supercharge Method Study Group. October 11, 1954
Splitter, 2016	Splitter D, Pawlowski A and Wagner R (2016) A Historical Analysis of the Co-evolution of Gasoline Octane Number and Spark-Ignition Engines. Front. Mech. Eng. 1:16. doi: 10.3389/fmech.2015.00016
Standard Oil Company, 1954	Standard Oil Company, Snell, J., Personal letter from Mr. Snell to the Members of the Supercharge Improvement Study Group. July 16, 1954.
Sunoco, 2020	Sunoco Race Fuels, "Race Fuel 101: Lead and Leaded Racing Fuels", https://www.sunocoracefuels.com/tech-article/race-fuel-101-lead-leaded-racing-fuels , accessed 06/20/2020.
Swarts, 2005	Swarts, A., Yates, A., Viljoen, C., and Coetzer, R., "A Further Study of Inconsistencies between Autoignition and Knock Intensity in the CFR Octane Rating Engine," SAE Technical Paper 2005-01-2081, 2005, https://doi.org/10.4271/2005-01-2081 .
Texas Company, 1955	The Texas Company, "Supercharged Method Knockmeter 103-A", Personal letter from Mr. Kulason to Mr. Snell and Members of the Supercharge Method Study Group. January 27th, 1955.
US Treasury Department, 1925	US Treasury Department. United States Public Health Services. "Public Health Bulletin No. 158. Proceedings of a Conference to Determine whether or not there is a Public Health Question in the Manufacture, Distribution or Use of Tetraethyl Lead Gasoline", Washington D.C., 1925.
US-Patent 2,269,760	K.R. Elredge, United States Patent 2,269,760, Detonation Indicator, Filed 1939. Granted 1942.
US-Patent 2,337,522	K.R. Elredge, United States Patent 2,337,522, Detonation Measurement, Filed 1943. Granted 1943.
US-Patent 2,448,323	D.R. De Boisblanc, United States Patent 2,448,323, Detonation Meter, Filed 1944. Granted 1948.
US-Patent 2,496,337	D.R. De Boisblanc, United States Patent 2,496,337, Detonation Meter, Filed 1944. Granted 1950.

US-Patent 2,633,738	D.R. De Boisblanc, United States Patent ,633,738, Detonation Meter, Filed 1948. Granted 1953.
US-Patent 3,289,461	P.E. Kahler, United States Patent 3,289,461, Detonation Meter, Filed 1963. Granted 1966.
WHO, 2020	WHO, "Exposure to Lead: A Major Public Healeth Concern", World Health Organization, Switzerland, 2010. https://www.who.int/ipcs/features/lead..pdf?ua=1 , accessed 06/20/2020.

Abbreviations

ACC	Accelerometer
°aTDC	Degrees After Top Dead Center
°bTDC	Degrees Before Top Dead Center
BDC	Bottom Dead Center
BMEP	Brake Mean Effective Pressure
CA	Crank Angle
CA10	10% Mass Fraction Burned
CA50	50% Mass Fraction Burned
CA90	90% Mass Fraction Burned
CFR	Cooperative Fuel Research
CRC	Coordinating Research Council
FMEP	Friction Mean Effective Pressure
HI _{BRF}	High Bracketing Reference Fuel
IMEP	Indicated Mean Effective Pressure
LO _{BRF}	Low Bracketing Reference Fuel

MAPO	Maximum Amplitude of Pressure Oscillations
MIC	Microphone
MON	Motor Octane Number
MRC	Most Representative Cycle
NEG	National Exchange Group
NO	Nitric Oxide
O ₂	Oxygen
ON	Octane Number
P _{Cyl}	Cylinder Pressure
PN	Performance Number
PRF	Primary Reference Fuel
RON	Research Octane Number
RPM	Rotations Per Minute
SI	Spark Ignition
TDC	Top Dead Center
TEL	Tetraethyl Lead
THC	Total Hydrocarbon
TPA	Three Pressure Analysis